Master of Science in Chemical Sciences Theses   Department of Chemistry and Biochemistry

Spring 5-10-2016

Novel Cell Penetrating Peptides Effect Endosomal Escape and Deliver Protein Cargos into Living Cells

Verra M. Ngwa
Kennesaw State University

NOVEL CELL PENETRATING PEPTIDES EFFECT ENDOSOMAL ESCAPE AND
DELIVER PROTEIN CARGOS INTO LIVING CELLS

by

Verra Manka'a Ngwa

B.S. Biochemistry

Kennesaw State University, 2014

_____

Submitted in Partial Fulfillment of the Requirements for the Degree of Master of Science
in the Department of Chemistry and Biochemistry
May, 2016

_____   _____
Committee Chair   Graduate Program Coordinator

_____   _____
Committee Member   Department Chair

_____   _____
Committee Member   College Dean

DEDICATION

This work is dedicated to Dr. John Salerno who conceived this idea of designing a new cell penetrating peptide. His passing away is an irreplaceable loss, but what he left with us is an unmeasurable blessing.

ACKNOWLEDGEMENTS

I would like to thank my thesis advisor, Dr. Jonathan McMurry, for teaching me everything I need to know to complete this thesis. With his guidance, I had the opportunity to explore more that was required and above my research. He continually allowed me do my work, but steered me in the right direction whenever he thought I needed it. I would also like to thank my committee members: Dr. Carol Chrestensen, for all that she taught me from tissue culture to cell biology and cell signaling; Dr. Scott Nowak, for the confocal work and for all the time spent time in the dark room acquiring microscopy images; and Dr. Salerno, for starting up this project.

In addition, special thanks to Allison Healey, for her unconditional support working on experiments and brainstorming together. To all the members of the McMurry lab, (past and present) for the friendly work environment we all shared. I want to say a big thanks to the entire faculty in the college of science with whom I interacted with on a daily based. And finally I would to thank my family for all their help and support especially their prayers.

ABSTRACT

Over the last decade a number of peptides that are rapidly internalized by mammalian cells have been discovered or designed. Cell-penetrating peptides (CPPs) are capable of mediating penetration of the plasma membrane, allowing delivery of macromolecular cargoes to the cell interior. We have developed a novel CPP-adaptor protein technology that allows any user-defined cargo delivery and release into the cytoplasm. Our hypothesis is that a CPP-adaptor with a moiety allowing high-affinity but reversible non-covalent cargo binding would lead to more efficient penetration and release than current CPP delivery strategies. Delivery of proteins to the interiors of cells has many applications. In addition to detecting and mapping the location of the components of living cells with fluorescent tags in real time, the availability of our system will likely enable the manipulation of signaling pathways and gene expression by allowing the introduction of components, e.g. constitutively active kinases, repressors or enhancers.

CPP-adaptor, TaT-Calmodulin, and cargo proteins (horse radish peroxidase, myoglobin and beta-galactosidase) were expressed and purified from E. coli BL21 (DE3)pLysS. Optical biosensing experiments demonstrated that affinity and kinetics between the novel CPP and cargo proteins did not significantly differ from wild-type interactions; all had subnanomolar affinities. Cargo proteins were labelled with DyLight 550. CPP-cargo complexes or cargo alone were incubated with subconfluent baby hamster kidney, HEK 293T and HT-3 cells. After washing, cells were imaged by fluorescence confocal microscopy. All users define cargos exhibited penetration and release to the cytoplasm whereas cargo-only controls exhibited no measurable penetration (though some adherence to the outside of the cells was observed). Time courses and dose-dependency studies characterizing penetration and release kinetics will be presented as will initial efforts to deliver cargo that may alter cell-signaling pathways.

The results presented herein demonstrate the feasibility of delivering a wide variety of cargo proteins to the intracellular environment; creating an array of potential research, diagnostic and therapeutic applications.

LIST OF TABLES AND FIGURES

TABLE OF CONTENTS

1. INTRODUCTION

1. INTRODUCTION

The plasma membrane of cells has a very selective barrier with regard to molecules of varying properties. This phospholipid bilayer is important for cell survival and function, but prevents the delivery of hydrophilic and other cargos such as therapeutic drugs, information rich molecules including oligonucleotides, genes, peptides or proteins *(1, 2)*. For example, oligonucleotides have therapeutic potential as pharmacological agents, but their high molecular weights and charge densities present a challenge for intracellular delivery*(3)*. It has also been a challenge for these hydrophilic molecules to cross the blood-brain barrier (BBB); a route that helps with the transport of therapeutic agents from the vasculature into the brain parenchyma *(1)*. To develop the technology of exogenous delivery of molecules into living cells, molecular transporters have been sought.

Several strategies have been developed to deliver therapeutic agents into cells across cellular membranes. Pharmaceutical carriers, such as nanospheres, nanocapsules, liposomes, micelles, cell ghosts, lipoproteins, and polymers have been used to deliver some therapeutic and diagnostic agents. Some of these carriers are nanometers in size and can be coated with polyethylene glycol (PEGylated) to form 'stealth' nanocarriers *(4, 5)*.The delivery with these carriers is based on passive accumulation in the pathological regions making it difficult for cargos to be efficiently delivered to the target location. Other delivery methods, transfection, have also been used to translocate macromolecules such as DNA. Transfection techniques include microinjection, electroporation and

liposome and viral-based vectors. The downsides with transfection techniques include low efficiency, high toxicity and poor specificity *(6)*. Transfection with DNA into cells to produce genetically modified cells has additional drawbacks including the need for transcription and translation, and the lack of control of intracellular concentration.

Viral vectors have also been used for intracellular delivery, but the introduction of a viral vector may cause an inflammatory reaction or an insertional mutation *(7)*. This is because viral genomes can integrate into the host genome randomly, which may disrupt tumor suppressor genes, activate oncogenes, or interrupt essential genes. Another disadvantage of this method is that a virus package has limited space for a foreign gene while maintaining infectivity. Viruses also disrupt the normal cellular functions of their hosts after they invade the cell. Viral proteins compete with host proteins hence destabilizing regular host protein–protein interactions *(8)*. For example the HIV-1 genome has three standard retroviral genes (*gag, pol,* and *env*) which in addition to the auxiliary genes (*vif, vpr, vpu,* and *nef*) and the 2 regulatory genes (*tat* and *rev*); engage in a wide range of interactions between the host's proteins and viral proteins *(8-10)*.

The discovery and characterization of HIV-I TaT protein gave insight on translocation of large and hydrophilic molecules into the cell with less toxicity and high efficiency. TaT was the first of many peptides now known as cell-penetrating peptides (CPPs) to translocate the plasma membrane. For the purpose of this project, we constructed CPPs-coupled adaptors for protein cargo delivery into the cell. CPPs and potential cargos are discussed in the next sections.

1.1. What are cell penetrating peptides?

CPPs are short peptides ranging between 5-30 amino acid residues. They have the capacity to ubiquitously cross cellular membranes with very limited toxicity through energy-dependent and/or independent mechanisms with specific receptors *(11)*. It is promising that CPP-mediated delivery of macromolecules *in vivo* will be successful because *in vitro* experiments show transport. CPPs occur naturally and can also be synthesized. Natural CPPs include : HIV-1 TaT peptide which was derived from the human immunodeficiency virus type 1 transcription activating factor*(2, 12, 13)*, Antennapedia (Antp$_{43-58}$), also known as penetratin, was obtained from *Drosophila Antennapedia* homeodomain transcriptional factor*(14-16)*, pVEC was from murine vascular endothelial cadherin *(17)*, buforin II was a histone-derived antimicrobial peptide *(18)*, and VP22 was from Herpes simplex virus (HSV) type I structural protein *(19-21)*. Oligoarginine peptides *(22, 23)*, amphipathic peptide *(24)*, and transportan *(25)* are some designed synthetic CPPs. Much precaution is required when designing CPPs in-order to avoid low yields, poor solubility, aggregation, or toxicity.

Since the discovery of the first CPPs, several different CPPs have been shown to deliver proteins, therapeutic drugs, nucleic and other cargos into the cell (Table 1). CPPs have gained attention in both medical and biological sciences not just because they can to internalize *in vitro* and *in vivo*, but also because of the potential for variable modification design *(26)*.

1.1.1. Classification of CPPs

The most common way to classify CPPs is based on origin, synthetic or natural. The natural CPPs are truncated versions of proteins and have been classified in subgroups depending on the chemical properties: cationic, amphipathic, and hydrophobic.

1.1.2. Cationic CPPs

Cationic CPPs are peptides with a high positive net charge because, they are rich in arginine and lysine. It has been suggested that at least six to eight positive charges are needed for efficient uptake of several cationic CPPs *(26, 27)*. Initially, cationic CPPs were used as delivery tools without any cellular response, but it was later discovered that they induced a wide range of side effects, including effects on membrane integrity and cell viability, which might be more subtle than cell death *(15, 26, 28)*.

1.1.3. Amphipathic CPPs

Amphipathic CPPs on the other hand are peptides which contain both polar and non-polar groups. The amphipathic nature of these peptides may evolve from the primary structure of the protein *(26)*. Amphipathic CPPs may be derived either from natural proteins such as pVEC or by covalent linkage of a hydrophobic domain to a nuclear localization signal sequence e.g MPG (table 1)*(26)*.

1.1.4. Hydrophobic CPPs

Hydrophobic CPPs only have non-polar residues and typically have low net charge. Part of the amphipathic CPPs, such as MAP (table 1) contains some hydrophobicity *(26)*.

Table 1: Classes of cell penetrating peptides *(26)*

Type	Name	Amino acid Sequence
Amphipathic	Transportan	GWTLNSAGYLLGKINLKALAA
	Pep-1	KETWWETWWTEWSQPKKRKV
	MPG	GALFLGWLGAAGSTMGAPKKKRKV
	pVec	LLIILRRRIRKQAHAHSK
	MAP	KLALKLALKALKAALKLA
	CADY	GLWRALWRLLRSLWRLLWRA
Cationic	Polyarginie	R8, R9 , R10
	Tat49-57	RKKRRQRRR
	Penetrtin (pAntp)	RQIKIWFQNRRMKWKK
	DPV3	RKKRRRESRKKRRRES
Hydrophobic	Pep-7	SDLWEMMMVSLACQY
	G3	RLSGMNEVLSFRWL

1.2. Objectives of this study

The goal of this thesis project was to develop an array of tools for intracellular protein delivery. The main objectives were to develop and optimize a new cell penetrating peptide adaptor. To test protein-protein interactions of the CPP-adaptor, TaT-CaM, with natural calmodulin proteins and recombinant calmodulin proteins. To test the new CPP-adaptor for the ability to deliver one or more cargo proteins into living cells. Achieving the above goals, would enable us to design, produce and screen alternate CPP constructs as time and resources allowed, utilizing CPP moieties of other penetrance modes, e.g. amphipathic, hydrophobic, cationic. A long term goal of the project will be to use the CPP-adaptor system to deliver a protein that alters cellular morphology, such as being able to deliver a tumor suppressor protein to cells lacking it, inducing senescence.

1.3. Novel CPP-adaptors discussed in this thesis

The CPP-adaptor, TaT-CaM, consists of the cell penetrating sequence from the HIV transactivator of transcription *(12)* fused to calmodulin, a calcium sensor

protein. The addition of calmodulin allows any cargo with a calmodulin binding site (CBS) to bind TaT-CaM resulting in a transducible entity. Before going into details in chapter 2 describing the construction of the CPP-adaptor, TaT protein, Antennapedia, Calmodulin and a naturally calmodulin protein, nNOS will be discussed briefly here.

1.3.1. Transactivation of Transcription (TaT) peptide

TaT is an early regulatory protein of the HIV-1 genome. The size of TaT varies from 86-104 amino acid residues in length and is encoded by two exons *(8, 29, 30)*. This transactivation protein contributes to the activation of viral and cellular genes. A double splicing mechanism occurs where TaT is split off the TaT mRNA transcript and this cytoplasmic TaT is directed into the nucleus by a nuclear localization signal where it activates the viral genome (Figure 1A) *(31)*. HIV-I TaT functions in chromatin remodeling, phosphorylation of RNA polymerase II that is involved in the transcription of the full-length viral mRNAs, transactivation of viral genes, and binding to a specific structure of HIV-I mRNA *(32-35)*. These functions are necessary for the HIV gene expression in which TaT is the activator that overcomes the cellular barrier of mRNA transcription *(8)*. TaT does this by recruiting cellular proteins which relieve the repression of the viral long-terminal repeat (LTR), thereby enabling the viral promoter to induce the expression of viral genes *(32)*. Other TaT functions include the upregulation of cytokines expression levels, the HIV-1 co-receptor CCR5 and the interleukin-2 (IL-2) receptor (CD25) in HIV-1-infected cells *(8)*. Upregulation of cellular genes by TaT induces effects such as apoptosis *(36)*.
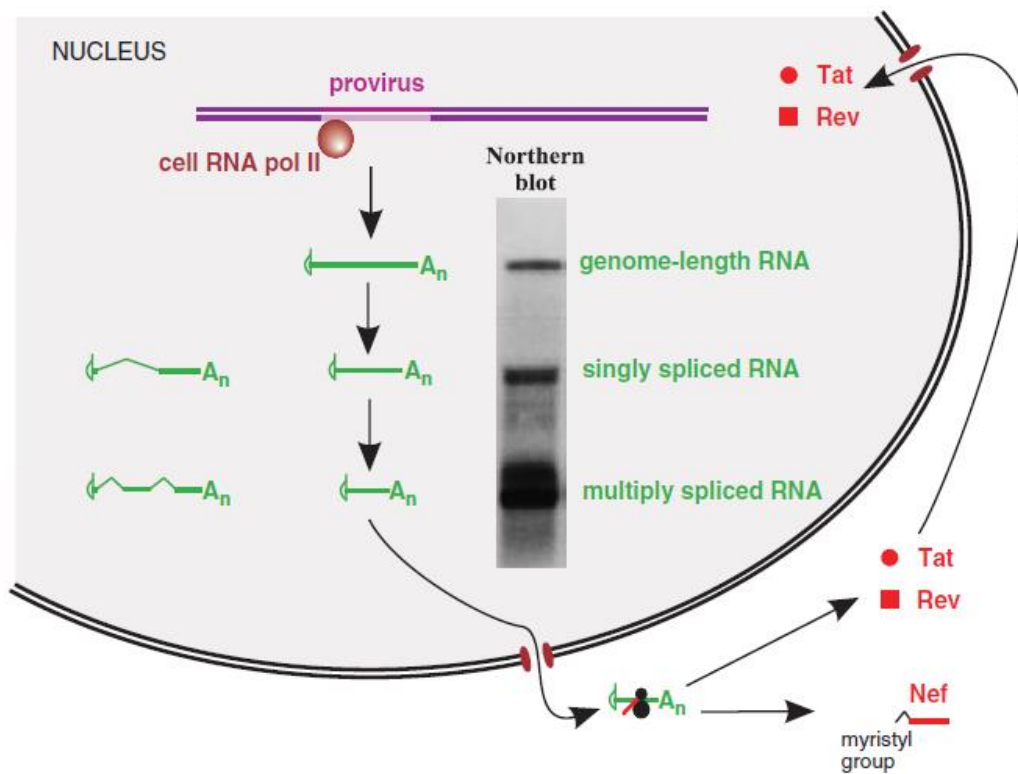
Figure 1A: *HIV-1 early gene expression.* Genome-length RNA is transcribed then much of it is spliced, giving rise to two further size classes of RNA that can be detected in northern blots of RNA from infected cells. Early in infection most of the RNA is multiply spliced and is transported to the cytoplasm, where the TaT, Rev and Nef proteins are translated. Nef is myristylated and performs a number of roles in the cytoplasm, while TaT and Rev are transported to the nucleus. Northern blot from Malim M.H. *et al*. (1990) *Cell*, **60**, 675.

Mutation studies have shown that only the 72 N-terminal residues are required for TaT functions in cellular internalization, and truncated TaT residues 48-60 from the protein transduction domain are responsible for internalization *(11-13, 37)*. $TaT_{48\text{-}60}$ region is made up of mostly basic amino acids, six arginine and two lysine residues (Table 1; Figure 1B). Arginine forms more stable hydrogen bonds with phosphoryl groups at physiological temperature due to its guanidinium group on the side chain *(38)*, and could also form stable interactions with the carboxyl, phosphoryl, and sulfuryl groups

on the cell surface, thereby facilitating endocytosis *(39)*. This positive-negative

interaction facilitates the initial entry step of TaT. Studies reveal that TaT_{48-60} peptide is

taken up by cells with concentrations as low as 1nmole and is not cell type specific *(13)*.

CD data and other physiochemical techniques confirmed the region of TaT covering 38–

49 domains has an α-helical structure with amphipathic characteristics *(40)*.
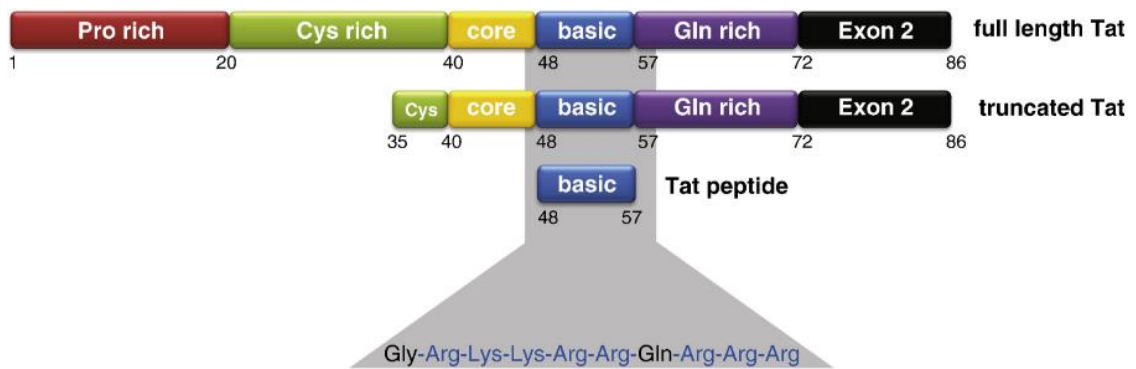
Figure 1B: The structure of full length TaT showing the basic arginine rich TaT_{47-57} peptide. The protein transduction domain consist of a basic domain with one amino acid from the central domain *(42)*

1.3.2. Antennapedia (Penetratin)

The antennapedia homeotic gene
is necessary for correct development of
thoracic segments in both larval and adult
stages of Drosophila. Loss of function of
this gene results in lethality in embryos or
larvae. The thoracic cuticle may also be
transformed into structures that are more
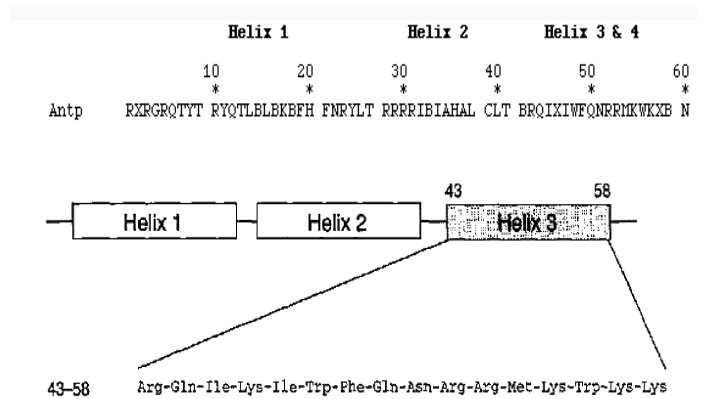
Figure 2: The 60 amino acids sequence of Antennapedia showing the third helix sequence from 43-58 *(46)*

8

anterior thorax or to the head *(41, 42)*. Cell developmental fate to some extent depends on the homeobox(antennapedia) protein. Homeodomain proteins like antennapedia are a class of transcription factors involved in many morphological processes that are from embryonic development to terminal differentiation. These family of proteins typically consists of three α-helices with one β-turn between helix 2 and 3 (figure 2) and bind to the DNA through a sequence of 60 amino acids *(15, 43)*. Through studies of the binding region of the homeodomain, the amino acids sequence has been shown to enter neuronal cells and translocate to the nuclei *(43)*. Mutation studies were able to identify the regions capable of this internalization, and have shown that a 16 amino acid sequence located in the third helix was responsible for translocation *(15, 44)*. It was for this reason that antennapedia was considered a cell penetration peptide.

1.3.3. Calmodulin

The primary adaptor used for the novel CPPs is this project is Calmodulin (CaM). Since TaT has been shown to translocate the plasma membrane, we coupled CaM to TaT forming TaT-CaM for protein cargo translocation. CaM is the major calcium-binding protein that binds and regulates a multitude of different protein targets in all eukaryotes *(45)*. CaM has the ability to bind up

Figure 3: Structure of free CaM (apoCaM) [A, shown by nuclear magnetic   resonance (NMR)] and bound CaM (Ca2+CaM) (B, shown by X-ray diffraction) *(119)*.

to four calcium ions (Figure 3 *(46)*, which induces a conformational change and renders CaM active and ready to carry out regulatory functions. The Ca^{2+}/CaM complex interacts

with many different proteins and might cause either activation or inhibition *(47)*. CaM mediates processes such as inflammation, metabolism, apoptosis, muscle contraction, intracellular movement, short-term and long-term memory, nerve growth, and the immune response. It can be expressed in many cell types and has different subcellular locations, including the cytoplasm, within organelles, or associated with the plasma or organelle membranes *(48)*.

We selected CaM because it is one of the most abundant, ubiquitous, and conserved proteins in eukaryotes *(46)*, which allowed us to hypothesize that it would be tolerated well. CaM binding sites are located within regulated proteins such that when it binds, it forces a conformational thus enabling or inhibiting the partner protein *(49)*. In the absence of calcium, the N-terminal domain of calmodulin is closed while the C-terminal is semi-open. In this case, the C-terminal might interact with some target proteins *(46)*, which may be why some proteins do not depend on the Ca^{2+}/CaM complex for activities e.g inducible Nitric Oxide Synthase (iNOS).

1.3.4. Nitric Oxide Synthase (NOS)

eNOS, nNOS, and iNOS are the isoforms of NOS that are responsible for nitric oxide (NO) released from L-arginine *(50-52)*. NO is a key determinant of endothelial function. It also functions as a neurotransmitter, a signal in skeletal muscle, an adaptive signal for developmental and growth of new blood vessels (angiogenesis) and a regulator of insulin control *(52)*. Studies have shown that eNOS and nNOS depend on Ca^{2+}/CaM for enzymatic activity *(50, 53)*. iNOS does not depend on Ca^{2+}/CaM for activation but rather on the genes encoding it at the level of transcription *(54)*.

NOS is active as a dimer and dimerization requires tetrahydrobiopterin (BH4), heme and L-arginine binding *(55, 56)*. Each monomer contains an N-terminal oxygenase domain and a C-terminal reductase domain. The oxygenase domain contains the substrate and BH4 binding sites while the reductase domain has the FAD, FMN, and NADPH cofactor binding sites *(55)* (Figure 4). The calmodulin binding site lies between the oxygenase and reductase domains. nNOS as a canonical calmodulin protein was first used to obtain preliminary data for this project. The binding kinetics of nNOS with TaT-CaM gave similar results as nNOS with wild type CaM *(57)*.
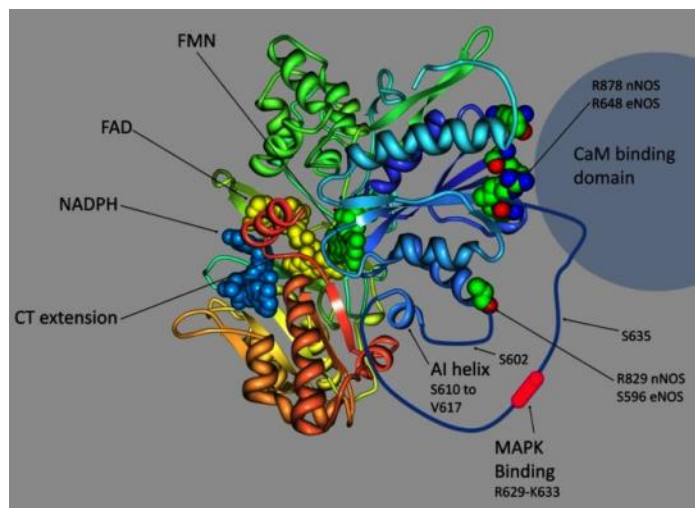
Figure 4: Structural cartoon of NOS reductase domains based on the nNOS reductase crystal structure. The FMN-binding domain is in blue, the FAD-binding domain green and the NADPH-binding domain is tan. Cofactors are shown in solid render and the residues at the N-terminal edge of the FMN-binding domain*(59)*

1.4. Calmodulin binding proteins expressed in *E.coli*

Recombinant CaM binding proteins that are expressed in *E.coli* were optimized as potential cargos for the new CPP-adaptor. *E.coli* is a robust, convenient, and inexpensive expression system for the production and purification of human proteins *(58)*. CPP-adaptor proteins and cargo proteins were expressed in BL 21 cells. These cells contain a T7 RNA polymerase gene integrated into the genome and are under control of the *lacUV5* promoter, a lactose analog (IPTG) inducible system. BL 21 (DE3) pLysis strains contained the plasmid that encode T7 lysozyme gene. T7 lysozymes inhibit T7 RNA polymerase hence reducing basal expressions of target genes. This provides a tight control of T7 RNA polymerase which is necessary when the recombinant protein to be expressed is toxic *(59)*. A list of CaM binding proteins that have been expressed in bacteria is shown in Table 2. Other cargos that we were interested in, but that lacked the CaM binding sites, were cloned into the vector pCAL-n-Flag *(60)* between BamHI and HindIII restriction sites.

Table 2: Calmodulin binding proteins

Cam binding proteins	Function	reference
NOS synthase	Catalyzes the production of NO from L-arginin	*(61, 62)*
Calcineurin	Regulate transcription faction NF-AT during T-cells activation	*(63-65)*
P68 RNA helicase	Involved in the processing of pre-RNA, rRNA, and miRNA	*(66, 67)*
Myosin light chain kinase	Phosphorylates myosin in the presence of Ca^{2+}/CaM thereby activating myosin so that it can interact with actin in smooth muscles	*(68, 69)*
Alpha spectrin	In red blood cells, it forms a meshwork that	*(69, 70)*

	supports the plasma membrane and defines the biconcave shape of the cell.	
Ribosomal protein L9	Encodes the ribosomal protein that is a component of the 60S subunits	*(71-73)*
Ribosomal protein S8	Primary binding protein that binds independently to the central domain of 16S rRNA and is required for proper assembly of the 30S ribosomal subunit	*(74, 75)*
P62	A putative RNA binding protein that may facilitate transport out of the nucleus.	*(76, 77)*
NAD kinase	Phosphorylates NAD to NADP. Both NAD/NADP in addition to being electron carriers, are also involved in process like signal transduction, transcription, DNA repair, and detoxification reactions	*(78, 79)*

1.5. Mechanisms of CPPs uptake

The mechanism of CPPs internalization remains a challenge even though a lot of studies have been done since the first discovery. Understanding the modes of translocation and intracellular delivery of cargos is an important step for optimization of the delivery systems. Biological and biophysical techniques have been used to follow up CPP penetration and cargo delivery into the cell. Several groups hypothesized that translocation occurs either by endocytosis or direct penetration of the peptide with or without its cargo (Figure 5). The mechanism used depends on the chemical and physical properties of the CPPs, the concentrations used, the biophysical properties, and the size of the cargo and the cell type it has to translocate *(5, 80)*.

13
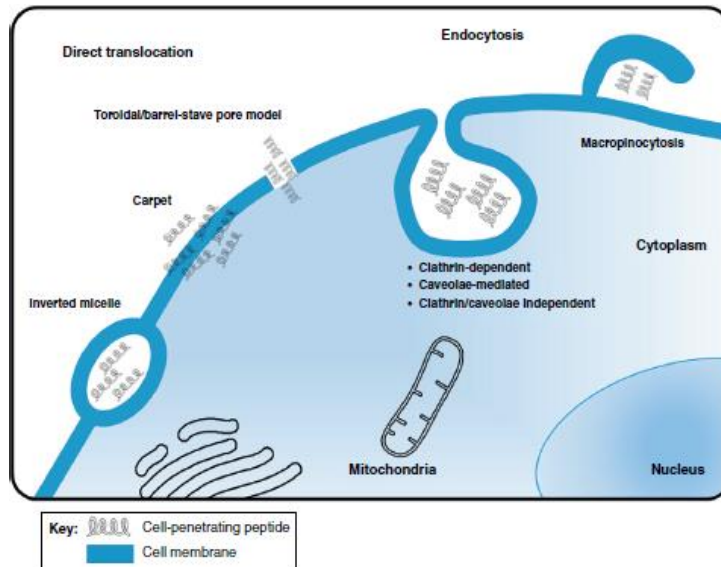
Figure 5: Intracellular pathways of cell entry for cell-penetrating peptides (CPPs)*(5)*

1.5.1. Direct penetration

Possible modes of CPP translocation through the membrane include; inverted micelle formation, pore formation, and the carpet-like model *(81)*.

*Inverted Micelle***:** This mechanism of uptake was first shown with penetratin *(82)*. This model involves the interaction of basic residues with the negatively charged phospholipids in the plasma membrane. Interaction destabilizes the bilayer, resulting in invagination of the membrane *(11)*. With the rearrangement of the neighboring lipids, inverted micelles are formed which encapsulates the peptide into the cell interior. Disruption of the membrane releases the peptide in the cell. Inverted micelle formations are highly favored with the presence of hydrophobic and bulky residues. Substituting tryptophan residues with phenylalanine inhibited formation of inverted micelles *(11)*.

The proposed mechanism of antennapedia states that the third helix associates directly to the membrane by electrostatic interactions *(15)*. The stability of this association enables the accumulation of the peptide on the membrane surface thereby enhancing the destabilization of the plasma lipid bilayer into an inverted micelle (Figure 6A) *(11)*, which then travel and finally open up on the cytoplasmic side.

Pore formation: Molecular dynamics suggest how TaT and arginine rich peptides translocate the phospholipid bilayer *(83)*. Interaction of the side chains of arginine and lysines from TaT peptide with the phosphate groups on the lipid bilayer leads to the accumulation of TaT in the outer leaflet of the bilayer. The bilayer becomes thin as a result of the peptide accumulation. The attraction between the positive side groups and the phosphate groups of the distal layer led to pore formation *(11)*.

Carpet-like model: This mechanism was first observed with cationic antimicrobial peptides that could penetrate into microorganisms leading to cell lysis *(84)*. Tryptophan promotes this mechanism. It is based on the accumulation of the peptide near the surface of the cell and at a higher concentration, which then penetrates the cell.
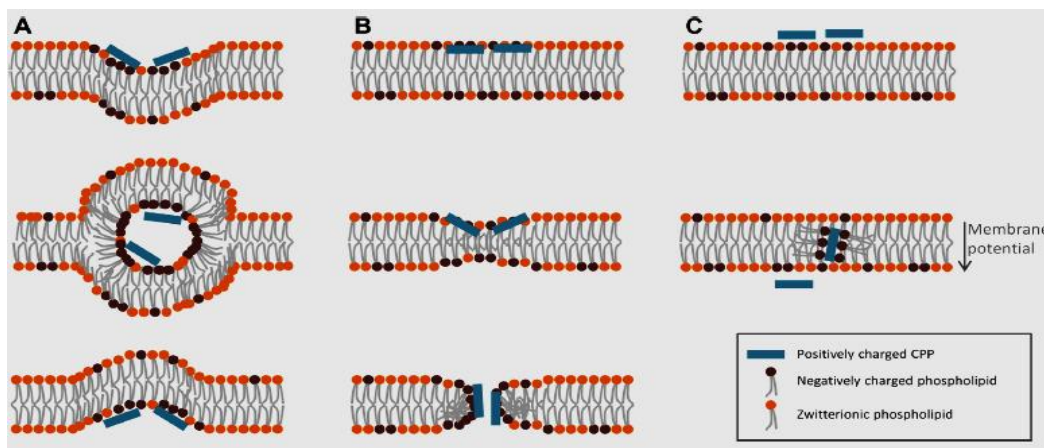
Figure 6: Proposed mechanisms for direct translocation: (A) Inverted micelle, (B) Pore formation, (C) Carpet like model *(86)*

1.5.2. Endocytosis pathways

Clathrin-mediated endocytosis, caveolin-mediated endocytosis, or clatherin/caveolae-independent endocytosis may also be mechanisms of CPPs uptake.*(5, 81)* To deliver macromolecules into cells through endocytosis, CPPs must possess certain characteristics. First, they must be able to associate with the cell surface. They must also stimulate and undergo efficient internalization via endocytosis. And finally, to be useful the CPPs must be able to deliver cargos across the lipid bilayer of the endosomal vesicles into the cytoplasm. This is likely the rate limiting step for intracellular delivery *(85)*. This pathway can include phagocytosis for the uptake of large particles and macropinocytosis for solute uptake.

Macropinocyhosis: This process consists of the inward folding of the outer surface of the plasma membrane directed by actin polymerization *(86)*. The invaginations result in the formation of macropinosome vesicles which are surrounded by membranes similar to the cell membrane. Dynamin is responsible for the membrane invagination *(81)*.

Clathrin-mediated endocytosis: This pathway takes up material into the cell with the clathrin-coated vesicles. This technique is used by all eukaryotic cells *(87)*. The functional unit of clathrin is known as a triskelion *(88)*. A triskelion is made up of three heavy chains and three light chains of clathrin. Interaction of several triskelia enables clathrin to self-assemble into a regular lattice. Clathrin mediated endocytosis involves five stages: initiation, cargo selection, coat assembly, scission and uncoating *(87)* in which clathrin molecules do not bind directly to the membrane or cargo receptors. Instead, they form vesicles by binding to membrane adaptor proteins, for example adaptin

protein 2 (AP2) *(88)*. At initiation, a membrane invagination pit is formed at the plasma membrane due to the presence of phosphatidylinositol (4,5)-bisphosphate *(87)*. Binding of the cargo to the receptor triggers the receptors to cluster together and a vesicle will start to form. Adaptin binds to the tail of the receptors on the cytoplasmic side of the cell and recruits clathrin. Clathrin then forms a shell around the coat. With the help of dynamin, the plasma membrane is cleaved and the coated complex is then release into the cell. The clathrin–adaptin complex falls apart and the cargo can then be transported to its destination in the cell. Clathrin recycles back to the plasma membrane to be used again.

Endocythosis via caveolin: Caveolae are round small invagination of the plasma membrane of about 50-80nm in diameter *(89)* and are enriched with cholesterol and sphingolipids. They are characterized by an integral membrane protein caveolin which hold the caveolae in the invagination of the bilayer membrane. Because the N and C terminals are present in the cytosol, a hydrophobic linker enables caveolin to be embedded into the plasma membrane.

Caveolae are involved in the internalization of membrane components such as glycosphingolipids, extracellular ligands like folic acid and albumin, bacterial toxins including cholera toxin and tetanus toxin, and non-enveloped viruses *(89)*. In this manner, bacterial and viruses can escape lysosomal degradation enabling use this pathway as a safer way for drug and DNA delivery *(90)*. Caveolae shape, composition, and function are cell type dependent *(89)*. They remain attached to the plasma membrane with the help of the actin cytoskeleton *(89)*. Cargos, for example the SV40 virus, have been shown to translocate by this pathway *(89-91)*. After binding to the plasma membrane virions are mobile until trapped by the caveolae. Once in the caveolae, the

ligand induces the activation of tyrosine kinases followed by a signaling cascade that results in slow but efficient internalization *(89)*. Phosphorylation enables the depolarization of actin filaments. Dynamin protein is then recruited which helps to pinch off the vesicle into the cell.

2 EXPRESSION AND PURIFICATION OF CPP-ADAPTOR PROTEINS AND CALMODULIN BINDING PROTEINS

2.1 TaT-CaM Expression

2.1.1 Construction of a vector encoding CPP-adaptor (TaT-CaM)

To generate pure protein for intracellular delivery, a protein expression vector was constructed. We modified the pET-19b vector with 6× His-tag for purification and TaT-CaM at the N-terminus as the CPP sequence. The gene of interest could easily be inserted into pET-19b using *Nde*I and *Bam*HI restriction sites, which facilitate the manipulation of various open reading frames (ORFs; Figure 7).

TaT

His -tag

Calmodulin
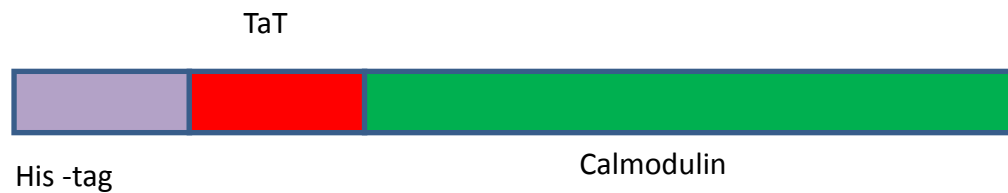
Figure 7: Schematic representation of recombinant TaT-CaM protein in pET-19b

2.1.2 Transformation of plasmid into Nova Blue competent cells.

We received 2μg of lyophilized plasmid containing the desired construct. The plasmid was then dissolved in elution buffer (10 mM Tris-HCl, pH 8.5 and 0.1 mM EDTA). Frozen competent cells were thawed on ice for 5 to 10 min. After addition of 50ng-100ng plasmid DNA to the competent cells, they were incubated on ice for 30minutes. The cells were then placed in a 42^0C heat bath for 1 minute and then incubated on ice for 2 minute. One ml of Luria-Bertani (LB) broth was added to the cells. The cells were incubated at 37 ^{0}C for 1 hr with shaking. The cells (100-150μM) were then plated on an ampicillin/tetracycline resistant LB agar plate and incubated overnight at 37 ^{0}C. The following day, an overnight culture was prepared by inoculating 5ml of LB medium with a single fresh colony followed by growing cells overnight at 37°C shaking at 220rpm. The cells were mini-prepped to create working DNA concentrations. All other constructs were treated the same way to ensure DNA stocks were not lost.

2.2 Ant-CaM Expression

2.2.1 Construction of a vector encoding CPP-adaptor (Ant-CaM)

The Ant-CaM plasmid was created in a similar fashion to that of TaT-CaM but the coding sequence was inserted into the pET-22b vector. The insertion was also between *Nde*I and *Bam*HI in an open reading frame.

Ant

His -tag   Calmodulin
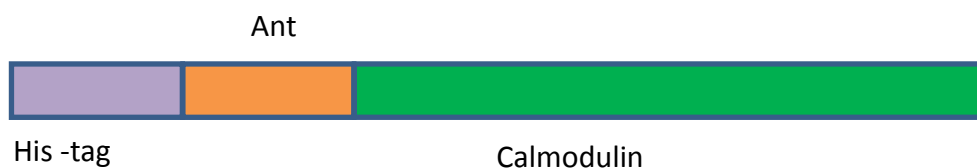
Figure 8: Schematic representation of recombinant Ant-CaM protein in pET-22b

2.3   TaT-CaM and Ant-CaM purification

The constructed vectors were transformed into BL21 (DE3) pLysS competent cells (New England Bio Labs) and cells were cultured in LB medium at 37^0C to an $OD_{600\,nm}$ between 0.4 and 0.6 absorbance. The cells were induced with 0.2 mM isopropyl-1-thio-β-D-galactopyranoside (IPTG, Sigma-Aldrich). Cells were harvested using a Sovall R 5C plus centrifuge at 7000rpm at 4 ^{0}C. TaT-CaM cells were resuspended in lysis buffer (10mM Tris-base pH 8.0, 10mM imidazole, 0.05% Tween, 500mM NaCl, 10% glycerol) in the presence of lysozyme and DNase using a vortex and a homogenizer. The lysis buffer used for Ant-CaM contained 8M urea because the protein was expressed in inclusion bodies. Hence, unless otherwise stated, all buffers (wash and elution) used for Ant-CaM contained 8M urea. The homogenized lysates were broken up using the French press.

The lysates were then separated into supernatant and lysate pellets by centrifugation at 18,000 rpm. Proteins in the soluble supernatant were purified by His-Tagged Talon metal affinity Resin (ClonTech laboratories, CA, USA) according to the manufacturer's instructions. Briefly, the resin was equilibrated in lysis buffer using a gravity column. The cleared lysates were incubated with the resin for 30min at 4^oC with

rocking. Protein-resin complex were washed with wash buffer (10mM Tris-base pH 8.0, 25mM imidazole, 0.05% Tween, 500mM NaCl, 10% glycerol) and eluted with elution buffer (10mM Tris-base pH 8.0, 250mM imidazole, 0.05% Tween, 500mM NaCl, 10% glycerol). TaT-CaM buffer exchange was performed on the FPLC while Ant-CaM was carried out using dialysis (2 changes with what difference in volume?which allowed the protein to refold.

2.4 Calmodulin-binding proteins (CBS-beta-galactosidase, CBS-horseradish peroxidase, CBS-myoglobin)

2.4.1   Human Beta-Galactosidase (β-gal)

β-gal is a lysosomal enzyme that cleaves the disaccharide lactose into glucose and galactose. After cleavage, these monosaccharides are able to be used in glycolysis. β-gal also catalyzes the transgalactosylation of lactose to allolactose *(92)*. In humans, this protein is encoded by the GLB1 gene and by the lacZ gene in bacteria. Any dysfunction or deficiency of β-gal will result in the accumulation of monosialotetrahexosylganglioside (G_{MI}) and keratin sulphate in cells leading to G_{MI} gangliosidosis and Morquio B metabolic disorders respectively *(93)*.

2.4.2   Horseradish peroxidase (HRP)

HRP is a plant secretory peroxidase that catalyzes the oxidation of various substrate including aromatic phenols, indoles, phenolic acids, amines, and sulfonates using H_2O_2 as the oxidant *(94)*. HRP exists as several isoenzymes in which the isoenzyme C1A is the most studied *(95)*. This isoenzyme contains a heme-group, two Ca^{2+} ions as prosthetic groups, and four disulphide bonds *(95)*. Thermal stability and

catalytic activities is enforced by the presence of Ca^{2+}. HRP has diverse functions in medicine including conjugation to antibodies. It is also important as a cancer treatment target *(95)*.

In this study, we used a truncated synthetic gene that encodes HRP-C1A. This truncated version lacks the heme group. This gene was used due to the difficulties in previous expression and purification of recombinant HRP in different expression systems *(96)*.

2.4.3   Myoglobin (Myo)

Myoglobin is a cytoplasmic hemoprotein that is expressed primarily in the skeletal and cardiac muscles. Myo was the first protein in which a three-dimensional structure was determined revealing its highly alpha-helix structure *(97, 98)*. Myoglobin functions as an oxygen storage hemoprotein- capable of releasing O_2 during periods of hypoxia or anoxia. Myoglobin also acts as a buffer to intracellular O_2 concentration when muscle activity increases and to facilitate intracellular O_2 diffusion by providing a path that increases simple diffusion of dissolved O_2. It has been a powerful scavenger of nitric oxide (NO) and reactive oxygen species (ROS). This implies that Myo might have a role in cell signaling in mammalian cells since ROS are mediators of cell signals *(98, 99)*. Myo was chosen not only because biochemically it has been highly study, but also to show the efficiency of our CPP-adaptor translocating both large and small molecules into the cell.

2.4 Construction of CBS-protein plasmid

We constructed the vector to express the CBS-proteins by inserting the genes into the pCAL-n-FLAG vector. The cDNAs of β-gal, HRP, and Myo were inserted between restriction sites BamHI and HindIII in an open reading frame (Figure 9)

A

CBS-Cargo

B
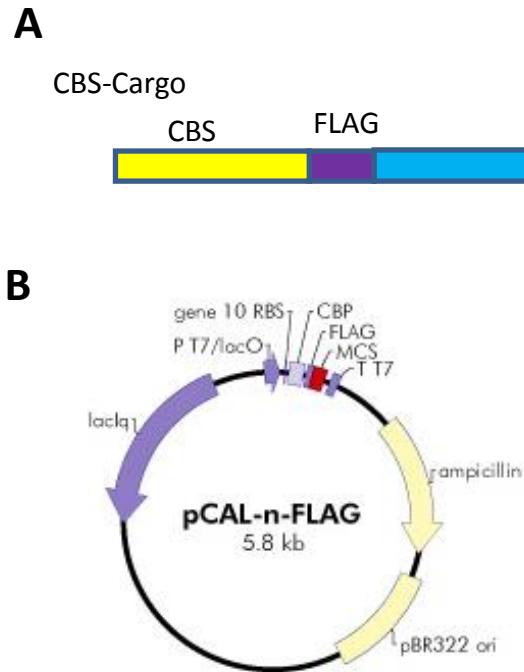
Figure 9: A) Schematic representation of recombinant CBS-Cargo proteins. **B)** Commercial plasmid with a calmodulin binding site (Addgene)

2.5 Expression and purification of CBS-proteins

The expression and purification of CBS-β-gal, CBS-HRP and CBS-Myo were similar to that of TaT-CaM described above. pCAL-n-FLAG vector encoding the CBS-proteins were transformed into BL 21(D3)pLsS. The cells were induced with 0.2mM IPTG for 4 hours at 30^0C. Cell pellets were lysed at room temperature in resuspension

buffer (50mM Tris-base, 150mM NaCl, 1mM EDTA, 1mM DTT, 10% glycerol; pH 7.8) with lysozyme and DNase using a vortex and a homogenizer. The homogenized lysate was French pressed to break up the cells. The soluble supernatants were purified over a calmodulin sepharose resin column on fast protein liquid chromatography (FPLC). The column was washed with equilibration buffer (50mM Tris-base, 150mM NaCl, 0.1mM DTT, 2mM CaCl2, 10% glycerol) to remove unwanted proteins. Proteins were eluted with elution buffer (50mM Tris, 0.1mM DTT, 150mM NaCl, 4mM EDTA, 10% glycerol). A buffer change was performed by dialysis in CBS buffer (10mM HEPES pH 7.4, 100mM NaCl, 1mM CaCl2, 10% glycerol) or using FPLC.

2.6 SDS-PAGE gel electrophoresis and Western blotting to confirm pure proteins

TaT-CaM, Ant-CaM and CBS-proteins samples were mixed with SDS-PAGE sample buffer (20%glycerol, 0.125M Tris-HCl buffer pH 6.8, 2% SDS,0.02% bromophenol blue) and 5% β-mercaptoethanol to avoid disulfide bridges formation to a final concentration of 1X. Mixed and denatured samples were heated in a 95^0C bead bath for 5mins. They were then loaded onto an SDS casting gel containing a stacking gel on top (5% polyacrylamide) and a resolving gel on the bottom (15% polyacrylamide). A constant current of 30mA was applied and the samples were allowed to run until they migrated to the bottom of the resolving gel. The gels were stained with Coomassie brilliant blue staining buffer (0.1% Coomassie blue R-250, 45% methanol, 10% acetic acid) and destained in Coomassie destaining buffer (45% methanol, 10% acetic acid).

Another set of samples from SDS-PAGE gel were transferred at constant voltage of 100V onto a nitrocellulose membrane by western blot. The membrane was blocked with 5% non-fat milk for 1hr and probed with 1:1000 anti-calmodulin (TaT-CaM and Ant-CaM) and 1:2500 rabbit anti-FLAG (CBS-proteins).

2.7 Results and Discussion

2.7.1   His–tag purification of TaT-CaM and Ant-CaM.

To confirm purification of TaT-CaM and Ant-CaM, the protein was analyzed via 15% SDS-PAGE gel and stained with Coomasie brilliant blue. Western blot probing with anti-calmodulin also confirms purification (Figure 9). TaT-CaM is expressed and purified as an active protein compared to TaT protein which is expressed in inclusion bodies *(100)*. The concentration of TaT-CaM and Ant-CaM were determined using Bradford assay.

Figure 10: Purification and detection of TaT-CaM (left) and Ant-CaM (right). Commasie brilliant blue stain (top). Western blot analysis for TaT-CaM (bottom) probed with 1:1000 anti-Calmodulin rabbit antibody
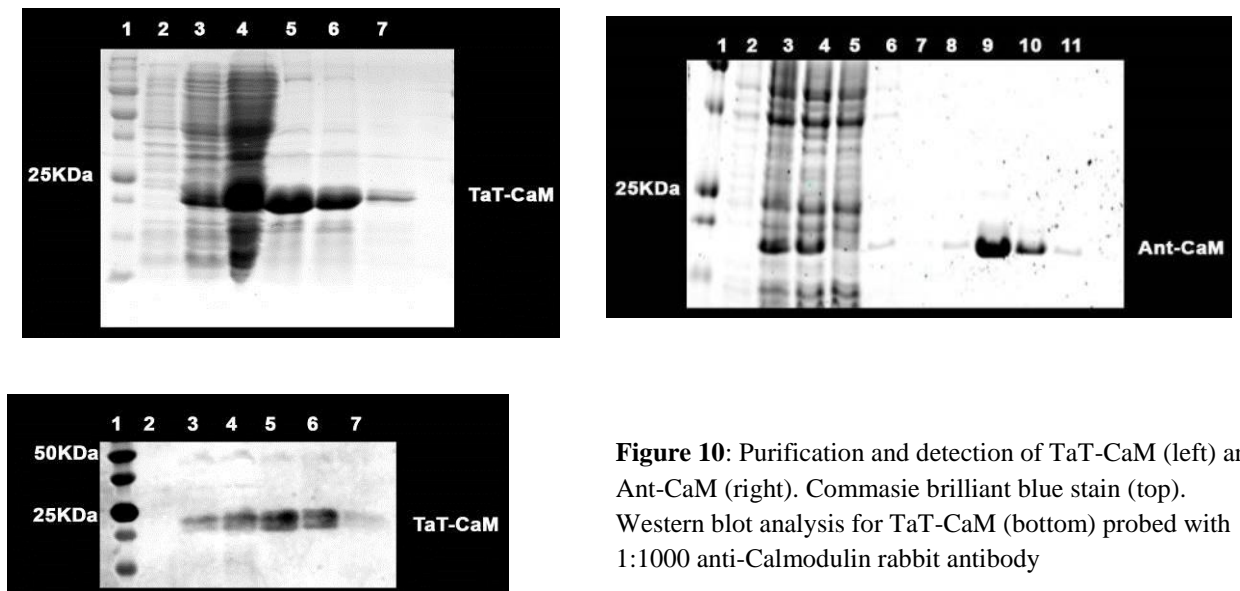
2.7.2 Expression and purification of calmodulin binding proteins.

CBS-β-Gal, CBS-HRP, and CBS-Myo were all expressed and purified from BL

9D3) pLysis cells. Western blot analysis was used to confirm purified proteins by probing

with monoclonal anti-FLAG mouse antibody (Sigma) (Figure 11).
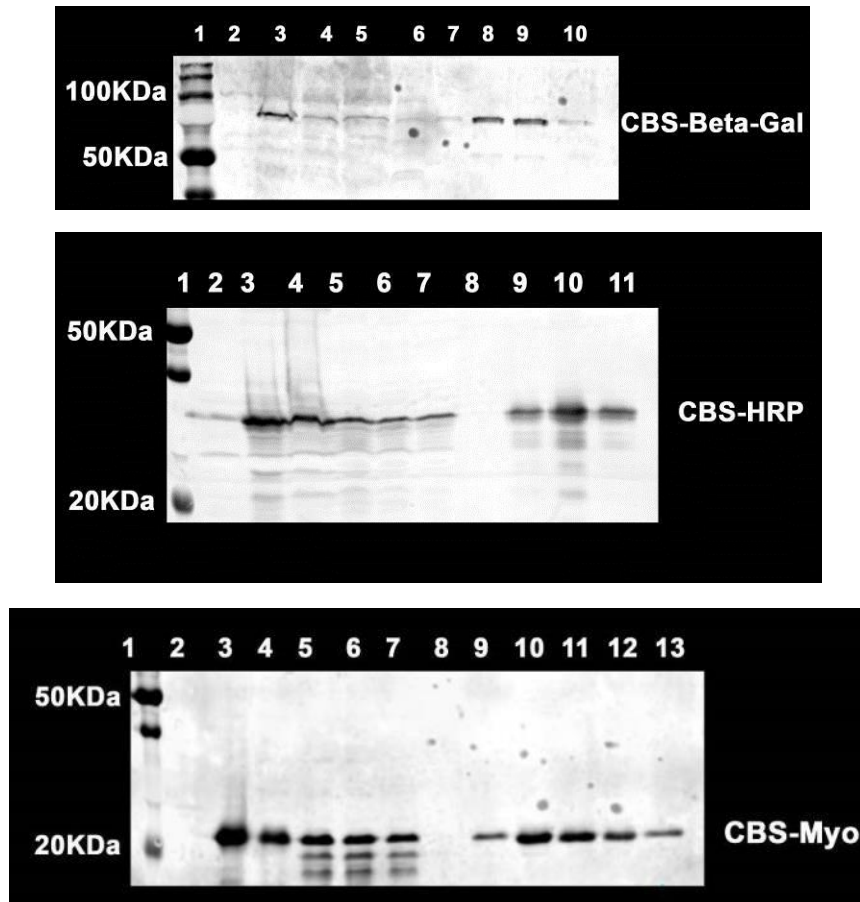
Figure 11: Purification of CBS-proteins, probed with 1:1000 anti-Flag mouse antibody.

2.8. Circular Dichroism analysis of wild type CaM, TaT-CaM and Ant-CaM

2.8.1. Introduction

To demonstrate that fusing the penetrating peptides TaT and Ant to CaM did not

alter the structure of CaM, we performed circular dichroism (CD) analysis on the purified

TaT-CaM and Ant-CaM with respect to wild type CaM (WT-CaM). CD is a

spectroscopic technique that is used to evaluate the secondary structure or conformational

of macromolecules, folding and binding of proteins in solution *(101, 102)*. CD measures

the difference in absorbance between left and right circular polarized light. The signal

from CD can either be positive or negative depending on which direction light is

absorbed the most. When the left circular polarized light is greater than the right circular

polarized light, CD signals are positive and negative to a lesser extent.

Secondary structures of proteins are determined in the far UV spectral region

(190-250nm). Within these wavelengths, the peptide bond is the chromophore, which

gives rise to a signal when located in a regular and folded environment while in the near

UV (320 -260nm), aromatic amino acid residue are observed *(102, 103)*. Analysis from

CD spectra gives the regular features of alpha-helices and b-sheets *(103)*. Alpha helix

proteins have negative bands at 222 and 208 nm and a positive band at 193 nm *(104)*

while beta-sheets have a negative band near 218 nm and positive band at 195 nm *(105)*.

Disordered proteins on the other hand have low ellipticity above 210nm and native bands

near 195nm *(106)*.

Protein characterization on CD requires that the protein be at least 95% pure on

SDS-page gel using Coomasie staining. Also, high quality CD data depends on the

protein concentration and the ionic strength of the buffer used. Calmodulin being a Ca^{2+}

sensor with the ability to bind up to four Ca^{2+} ions induced a conformational change *(45, 57, 107)* is made up of highly alpha helix structure. CD analysis showed that in the presence of Ca^{2+}, the negative alpa-helix peaks are deeper at 222nm and 208nm than in the absence of Ca^{2+}*(87, 108)*. We analyzed the structures of TaT-CaM and Ant-CaM using the self-consistent method (SELCON).

2.8.2. Methods and material

All CD experiments were carried out using a JASCO J-710 Spectropolarimer (JASCO Inc., Tokyo, Japan). Measurements were recorded over wavelengths of 196-250 nm in a 0.1 cm path length cell with a scanning speed of 10nm per minute. Temperature was controlled at $25^{o}C$ using a water bath. All samples analyzed were dialyzed into 10mM HEPES (pH 7.4) containing 100mM NaCl, 1mM CaCl2, 0.1% Tween, and 10% glycerol. The proteins concentrations were adjusted to a final concentration of 0.25mg/mL in the absence of EDTA and 0.25mg/mL in the presence of 5mM EDTA.

2.8.3. Results

The CD spectra of wild type CaM has previously shown peaks in the far UV region between 195-250nm *(87, 101)*. Comparing the spectra of Ant-CaM and TaT-CaM with respect to that of wild type CaM, we observed similar patterns with all three peptides in the absence and presence of EDTA. (Figure 12).

Table 3: Alpha-Helix content of CAM, Ant-CaM and TaT-CaM

		Without EDTA	With EDTA
CaM	α-Helix	22%	23%
Ant-CaM	α-Helix	20%	23%
TaT-CaM	α-Helix	18%	15%
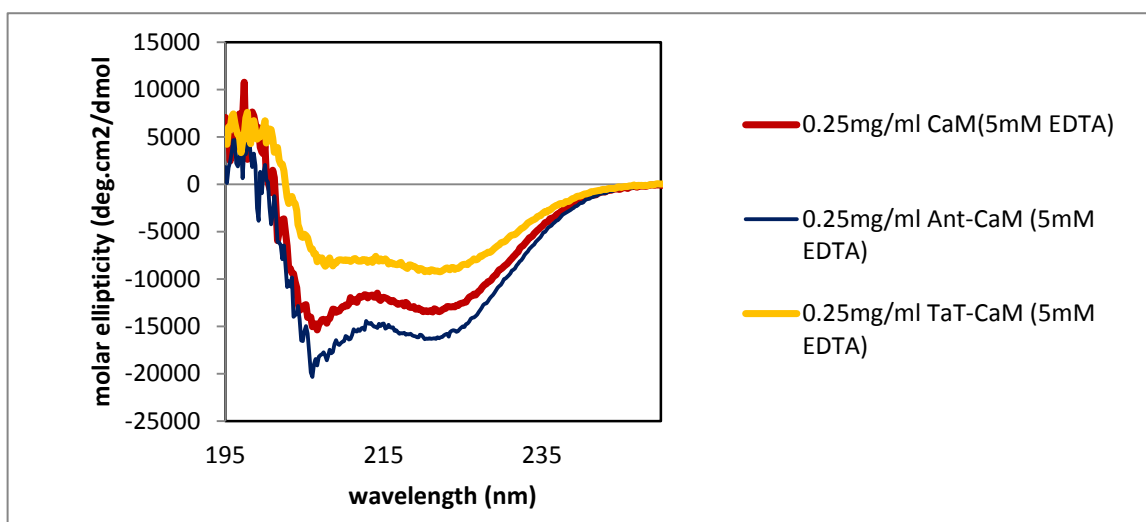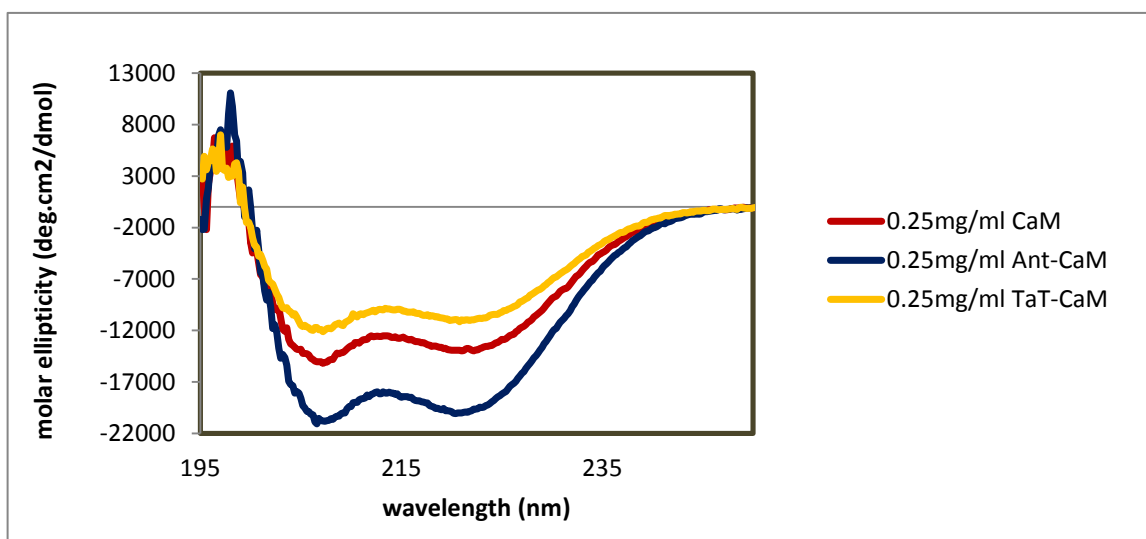
Figure 12: CD spectra of wild-type CaM, TaT-CaM, and Ant-CaM. Without EDTA (Top plot); with 5mM EDTA (Bottom plot)

Using SELCON3 method, we deduced the alpha helix structures of CaM, Ant-CaM, and TaT-CaM. In this method, the spectrum of the protein analyzed is presented base on the spectrum of the reference protein having the CD spectrum similar to the unknown protein. The reference set used for this analysis included in the far UV-region was SP43 (190nm-240nm).

The results obtained from these measurements showed that in the presence of Ca^{2+}, alpha- helix structure is enhanced. In the presence of calcium the negative peak obtained at 222nm and 208nm were deeper than those obtained in the absence of calcium. These results confirmed that there is not a significant difference between the WT CaM and the CPP-adaptors. In the presence of Ca^{2+}, TaT-CaM and Ant-CaM spectras are the same as that of CaM. The disparity of the lines not overlaying is due to protein concentration. Bearing in mind that the Bradford test only gives an estimate of protein concentration, a better concentration would have been known if determined by another technique like quantitative amino acid analysis *(101)*. In the absence of Ca^{2+}, it is observed that the helix structures are less deep than in the presence of Ca^{2+}. The average alpha-helix from the regular and the distorted protein are very similar to each other in the absence and in the presence of EDTA. Therefore Ca^{2+} enhances the alpha-helix peaks.

2.9. **Summary**

Recombinant CBS-proteins were constructed into pCAL-n-FLAG plasmid, while recombinant TaT-CaM was constructed in pET19b and Ant-CaM in pET-22b. Both CPP-adaptor proteins and CBS-proteins were expressed at 30 ^{o}C in *E. coli* BL21 (BDP) using Luria Broth medium. Proteins expression was induced using IPTG. CBS-proteins were

purified by affinity chromatography (Calmodulin sepharose resin) and His-tag for Tat-CaM and Ant-CaM. Purified proteins were identified using Coomasie blue stain dye and Western blot probing for anti-Flag (CBS-proteins) and anti- Calmodulin (TaT-CaM). Starting with a liter of culture, the yield of 1ml f TaT-CaM yield was ~16mg while CBS-proteins were ~2.0mg. CD analysis further confirmed that covalently linking TaT and Ant penetrating sequences to calmodulin did not modify the secondary structure of calmodulin.

3. BIOLAYER INTERFEROMETRY AND CELL PENETRATION ASSAY OF CBS-PROTEINS WITH TAT-CAM

3.1. Biolayer Interferometry

Biolayer interferometry is a biosensing technique that operates in real time. One molecule, the ligand is tethered at the tip of the optical biosensor. White light travels down to the molecule and reflects off. The interference pattern is measured as a shift in wavelength (Figure 13A). Once a baseline has been established, the senor is then moved into an analyte containing buffer to monitor association and finally moved into an analyte free buffer to measure dissociation. Binding of both the ligand and the analyte on the sensor increases the reflecting surface hence causing a coincident change in the interference pattern (Figure 13B and Figure 13C) *(109)*
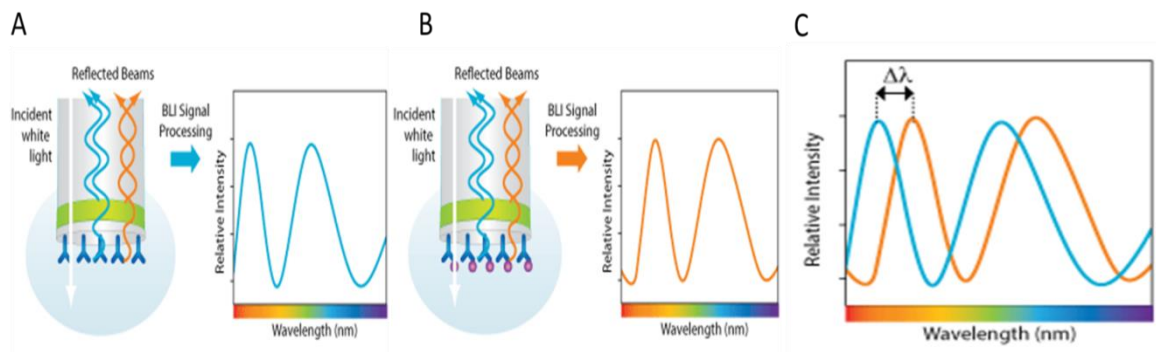
Figure 13. The biolayer interferometry principle. A) An interference pattern is established by reflection of white light from two surfaces on a fiber optic sensor with biotinylated molecules attached to the biolayer. B) Binding of analyte molecules causes a shift in the wavelength of the interference pattern. C) Monitoring of the interference shift over time reflects association of analyte with the immobilized molecule. Association is measured in the presence of analyte and dissociation is measured when the sensor is moved to buffer containing no analyte. *(110)*

BLI measurements were performed on a FortéBio Octet QK biosensor using streptavidin sensors (SA). Assays were performed in black 96-well microplates at 25^0C. All volumes were 200µL. TaT-CaM was biotinylated using NHS-LC-LC-biotin (succinimidyl-6-[biotinamido]-6-hexanamidohexanoate) (Thermo Scientific, Rockford, IL, USA) at a 10:1 molar ratio of biotin to protein for 30 min at 25^0C. Free dye was separated from reactive biotinylated TaT-CaM by rapid buffer exchange over a desalting column. After loading biotinylated TaT-CaM onto SA sensors, a baseline was established in NOS binding buffer prior to association at varying analyte (CBS-proteins) concentrations. Dissociation was subsequently measured in buffer only and buffer with 10mM EDTA.

3.2. Cell penetration assay of TaT-CaM with CBS-proteins in BHK 21, HEK 293T, HT-3 cells by confocal laser scanning microscopy

3.2.1. Confocal Laser Scanning Microscopy (CSLM)

Confocal Laser Scanning Microscopy (CLSM) is a technique used to obtain sharp images over a narrow depth of field. This is accomplished by eliminating most of the light from the specimen out of the microscope focal plane. This technique makes it possible to take thin sections from the sample and build up a two or three-dimensional image along a vertical axis, a process known as optical sectioning. Confocal laser scanning microscopy depends on point illumination with a focused laser and a pinhole detector that rejects out of focus light allowing just the focal point of the sample to be

detected. When the point illumination excites fluorophores in a region on the sample, out of focus light is removed by the pinhole detector producing a sharp confocal point *(110)*.

Photons emitted from the sample are detected by a photomultiplier tube and are analyzed by a computer. An important role of confocal microscopy is the ability to distinguish between intracellular and extracellular fluorescence without the removal of fluorescent medium; hence, it can be used to qualitatively evaluate the internalization and distribution of CPPs in cells.

3.2.2. Cell culture

BHK 21 ATCC cells: Cells were removed from liquid nitrogen storage and placed in a 37^0C bead bath for 2min and then closely monitored until they thawed. The cells were transferred into a 15ml conical containing 5ml Dulbecco's modified Eagle's medium (DMEM) with 10% fetal bovine serum (FBS). Cells were centrifuged for 5min at 1000 rpm at 30^0C. BHK 21 cells were re-suspended into 12ml pre-warmed growth media at 37^0C and 5% CO_2, and then transferred into a T-75 flask. Cells were then returned into the incubator at 5% carbon dioxide atmosphere, 37^0C.

Subculturing BHK cells: Cells are maintained as they grow. When cells were maximally between 80-90% confluent in a T-75 flask, the culture medium is removed and discarded. The cell layer was quickly rinsed with 0.25% (w/v) Trypsin 0.1%EDTA solution to remove all traces of serum which contains trypsin inhibitor. Trypsin-EDTA solution (3ml) was added into the flask and placed in the 37^0C incubator for 5min and dispersed cells were observed under a light microscope. Growth media (6ml) was added into the T-75 flask and the mixture was pipetted gently to mix. The cells in suspension were then transferred into a 15ml conical tube and centrifuged for 5min at 1000rpm using

a bench top (Eppendorf 5702HS) centrifuge. Cell pellets were resuspended into 10ml of growth media and aliquots added into new culture flasks and also in chamber Lab-Tek cover glass for penetration experiments.

Fluorescently labeled cargos: CBS-proteins were labeled with Dylight amine-reactive dye 550 according to the manufacturer's protocol (Thermo scientific). Briefly, purified protein (250ul to 500µl) was added into a 50µg dye tube pipetting up and down then vortexing gently. The mixture was incubated in the dark for 1 hour; then the dye removal column was used according to the Thermo scientific protocol. This removed the unreactive dye from the sample. Labeled proteins were aliquoted and stored at -80°C for future use.

Penetration assay: BHK 21 cells were seeded at 1.2×10^4 cells/ml in a 2-well Lab-Tek chambered cover glass (Fisher Scientific) in DMEM medium supplemented with 10%FBS and cultured overnight. The medium was discarded and replaced with fresh medium. The experimental chamber was treated with TaT-CaM and CBS-cargo at a final concentration of 1µM each while the control had only CBS-cargo. The chamber culture plate was incubated for 1 hour at 37^{0}C in a 5% CO_2 atmosphere. Cells were rinsed three times with PBS containing calcium and magnesium. The cells were treated with 2 µM cell tracker green dye (Thermo Fisher) for 20 min with incubation followed by three rinses with PBS. Cells were stained with a drop of NucBlue for 10min at 37°C. After two washes with PBS, DMEM/10% FBS medium containing 25mM HEPES pH7.4 buffer was added into the chambers. Penetration was analyzed using confocal microscopy.

3.3.   Results and Discussion

3.3.1. BLI assay with TaT-CAM

BLI measurements were performed to analyze protein-protein interaction between TaT-CaM and nNOS, and CBS-cargos. Biotinylated TaT-CaM was tethered to the SA sensor. After establishing a baseline in buffer only, the immobilized ligand was dipped into analyte containing buffer to monitor association and then moved to analyte –free buffer to monitor dissociation. Interference pattern over time is reported as a wavelength shift in nanometer. The wavelength shift results in molecules associating and dissociating from the tip of the biosensor. These real-time experiments enable label-free analysis for determination of affinity, kinetics and concentration of the analytes. Association and dissociation experiments are shown in Figure 14 along with simulation fits.

TaT-CaM was first examined for interaction with a natural calmodulin-regulated protein, nNOS. The binding affinity observed was similar to that of wild type CaM and nNOS as reported (*56)* when analyzed with biolayer interferometry. Designing and synthesizing new cargos with CaM binding sites: CBS-Myo, CBS-HRP, and CBS-β-gal, the binding affinity and kinetics of these protein-protein interactions were also determined. All CBS-cargos bound CaM with low nanomolar affinity and had expected fast-on, slow off kinetics (Figure14A-C). TaT-CaM and cargo proteins dissociated rapidly upon exposure to EDTA ($k_{off} \sim 0.1$ s^{-1}, Fig. 14E), indicating that the TaT-CaM-CBS interactions function essentially indistinguishably from those of wild type CaM. All analytes exhibited negligible binding to sensors without TaT-CaM. Rate and affinity constants determined from single-state global fits are listed in Table 4.

Table 4: Dissociation Rate constants

	K_D (nM)	k_{on} (M^{-1} s^{-1})	k_{off} (s^{-1})	k_{off} (EDTA) (s^{-1})
nNOS	15	$1.2 * 10^4$	$1.8 * 10^{-4}$	ND
CBS-β-Gal	73	$9.2 * 10^3$	$6.7 * 10^{-4}$	0.05
CBS-HRP	160	$1.7 * 10^3$	$2.8 * 10^{-4}$	0.2
CBS-Myo	0.9	$5.9 * 10^4$	$5.5 * 10^{-5}$	0.09
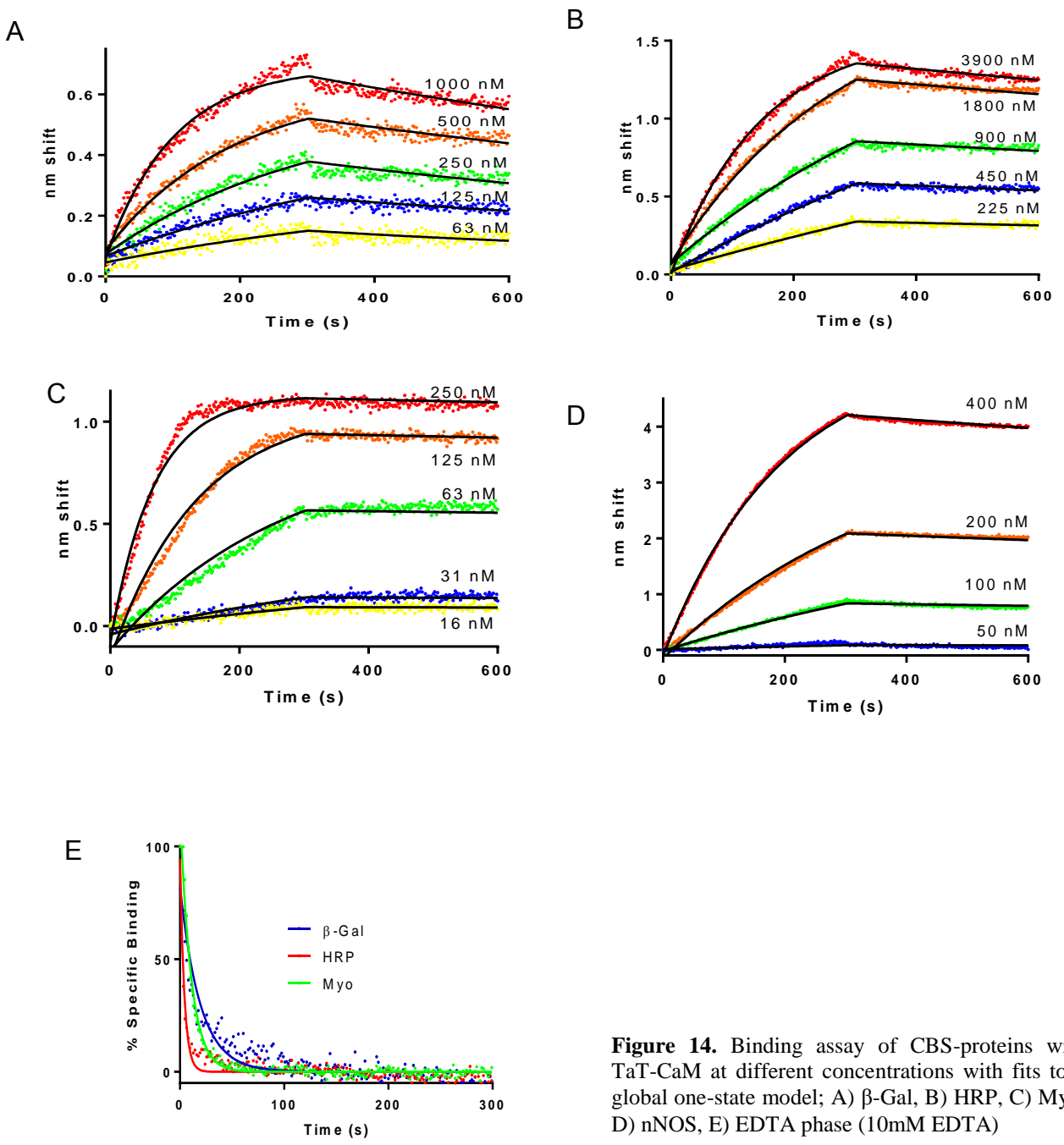
Figure 14. Binding assay of CBS-proteins with TaT-CaM at different concentrations with fits to a global one-state model; A) β-Gal, B) HRP, C) Myo, D) nNOS, E) EDTA phase (10mM EDTA)

3.3.2. BLI assay with Ant-CaM

Purifying Ant-CaM from inclusion bodies using 8M urea, the urea was removed slowly by dialysis to allow refolding.CD analysis showed the alpha helical structure of the protein when compared with wild type CaM indicating that the protein folded properly after dialysis. Optical biosensing experiments similar to TaT-CaM were performed between Ant-CaM and a nNOS splice variant $nNOS_{mu}$. AnT-CaM was the biotinylated ligand while $nNOS_{mu}$, the analyte. $nNOS_{mu}$ is expressed in skeletal muscles and has similar catalytic activity as nNOS expressed in the cerebellum *(111)*. $nNOS_{mu}$ binds CaM with low nanomolar affinity ($K_D = 3.1x10^{-9}$ M) and expected fast on ($K_{on} = 28303M^{-1}S^{-1}$) and slow off rate constants ($8.975x10^{-5}S^{-1}$) (Figure 15A and B). This complex rapidly dissociated when moved into 10mM EDTA (Figure 15C). The dissociation in EDTA is well defined due to the hydrophobic residues present in the anntenapedia penetration sequence (RQIKIWFQNRRMKWKK). Cell penetration studies have not been done using Ant-CaM.
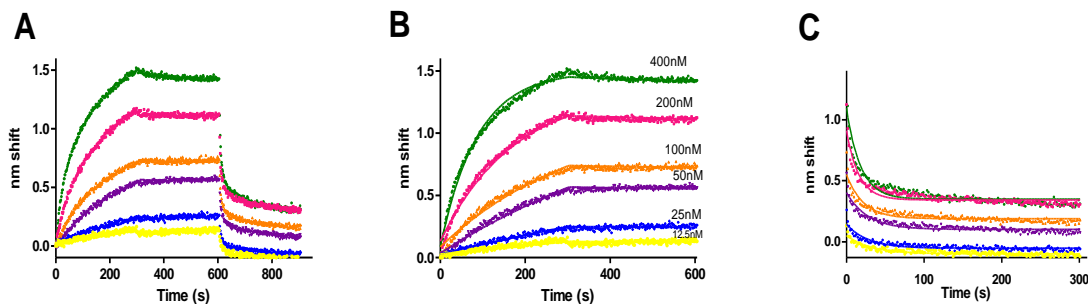
Figure 15: BT-Ant-CaM (ligand) interacting with nNOS mu (analyte). nNOS mu concentrations from top to bottom were 400nM (green), 200nM (pink), 100nM (orange), 50nM (purple), 25nM (blue), 12.5nM (yellow). **(A)** Full characterization of nNOS mu binding BT-Ant-CaM. **(B)** Association and dissociation phase. **(C)** nNOS mu in EDTA.

3.3.3. Cell penetration assay in BHK21, HEK 293T, HT-3 cells

As a preliminary measure of the ability of TaT-CaM to mediate uptake of cargo, neuronal nitric oxide synthase was labeled with Dylite 550 fluorophore and added to BHK 21 cells in the presence and absence of TaT-CaM. The cells were washed after one hour. Confocal microscopy showed that in the absence of TaT-CaM labeled nNOS aggregates were confined to the surface of cells and to the surface of the microscope slide. TaT-CaM mediated the uptake of almost all the labeled nNOS in less than an hour. Initially, internalized nNOS was contained in endosomes that appeared to move toward the nucleus over the next two hours (Figure 16). Considering the fact that nNOS is a large protein that is difficult to express and purify in *E.coli* and is very unstable hence cannot be stored for long term use; we designed, optimized, and synthesized proteins with calmodulin binding tags.

The initial proteins were chosen in order to show different characteristics ranging in size, oligomerization and structure. Uptake of cargo into cell interiors was assayed using an inverted Zeiss (Jena, Germany) LSM700 confocal microscope equipped with a 40x EC Plan-Neofluar objective (NA= 1.3). Z-stacks of both TaT-CaM treated and untreated cells were acquired and analyzed for incorporation of fluorescently labeled cargo into the cytoplasm. Orthogonal projections of Z-stacks were generated using Zeiss ZEN software, which allowed for viewing both treated and untreated cells alike at the same depth within the cell relative to the diameter of the nucleus. In the presence of TaT-CaM, all cargo proteins were delivered to the interiors of the cells and showed significant cytoplasmic distribution, indicating efficient penetration and escape from endosomes.

The fluorescently labeled cargo proteins without TaT-CaM showed a very small degree of adherence to the surfaces of cells, but no penetration into the cell as observed by absence of fluorescence at the same cytoplasmic depth as that observed in cells treated with TaT-CaM (Figure 17 -BHK21) and Figure 18 (HEK 293T and HT-3 cells).
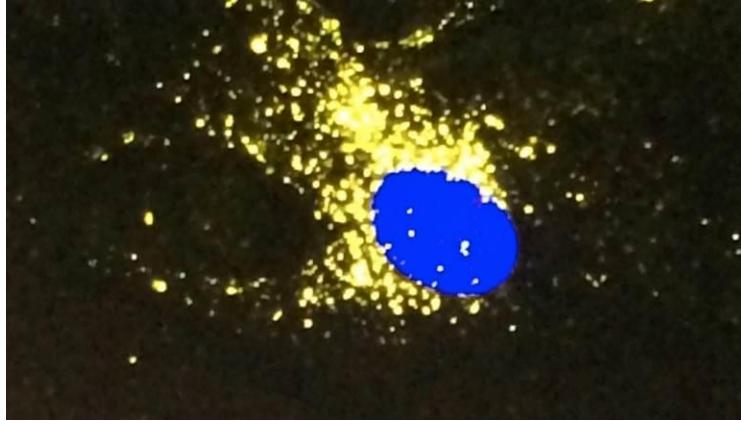
Figure 16: Projection confocal image of labeled nNOS 3 hours after the onset of TaT-CaM mediated uptake by BHK21 cells**.** Nucleus is stained blue; endosomes stained with labeled nNOS in yellow. Cytoplasm is stained by released nNOS. 3D cross sections confirm that labeled nNOS is inside the cells.
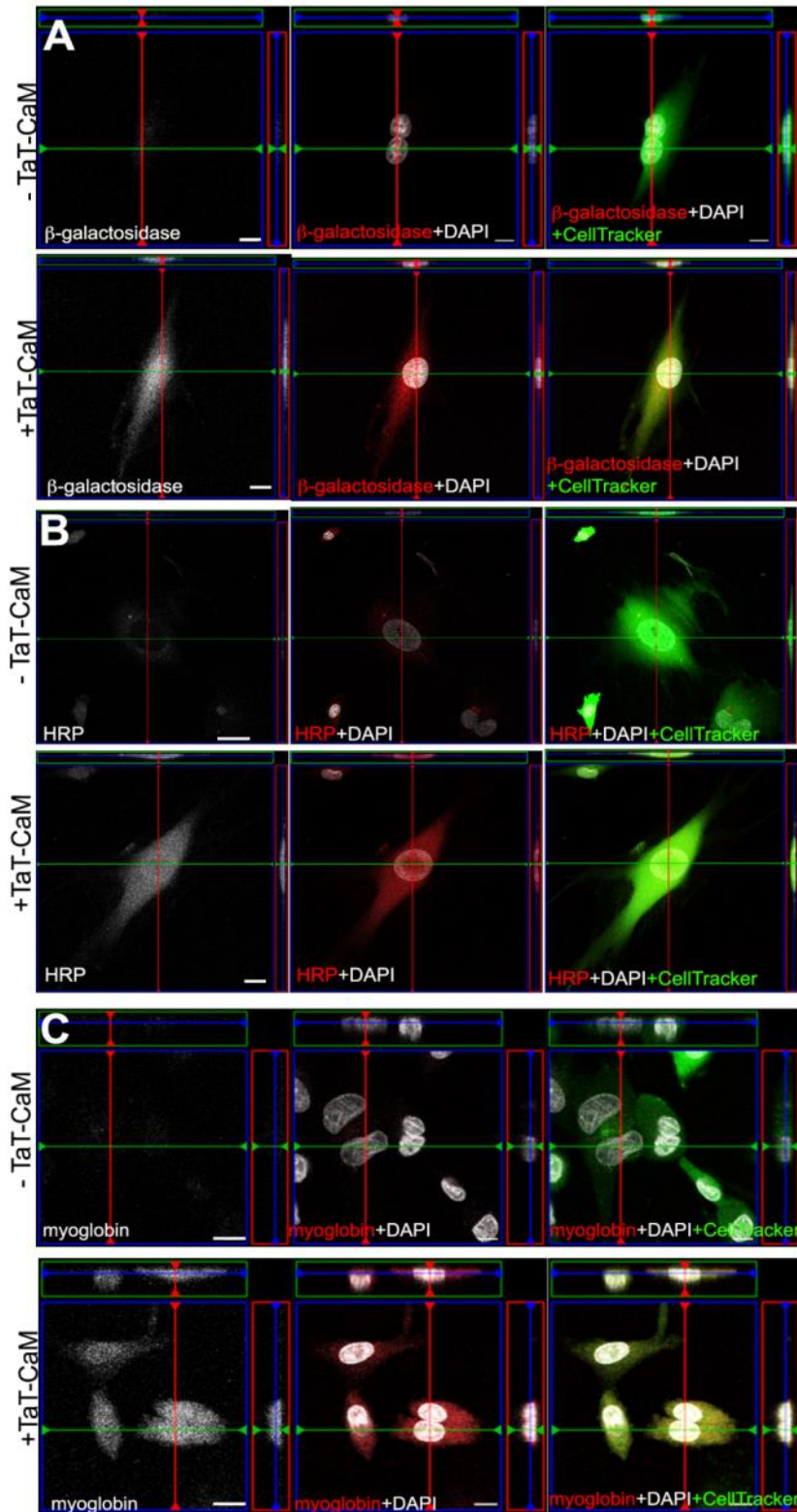
Figure 17: Confocal imaging of cell penetration. BHK cells were treated for 1 hour with fluorescently cargo proteins labeled with DyLight 550 (white in left panel, red channel in middle and all three channels in right panel), in the absence or presence of TaT-CaM. Cells were washed and imaged live. Orthogonal projections were generated and the center images presented are optical sections set at a similar depth of the nucleus (NucBlue staining, white, right panel), as determined by position within the Z-stack. Scale bars in all panels = 20 μm
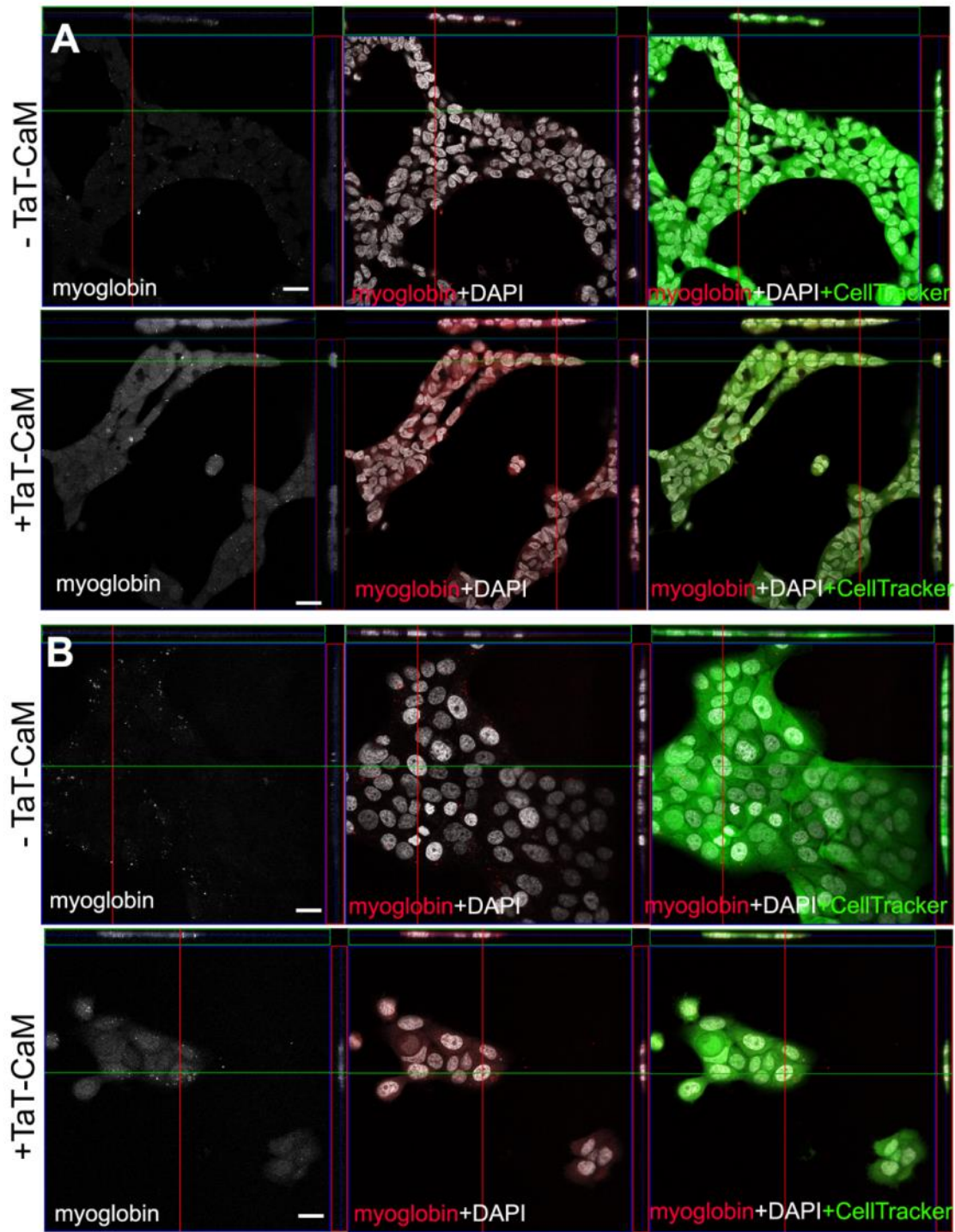
Figure 18: Confocal imaging of cell penetration. HEK 293T and HT-3 cells were treated for 1 hour with fluorescently cargo proteins labeled with DyLight 550 (white in left panel, red channel in middle and all three channels in right panel), in the absence or presence of TaT-CaM. Cells were washed and imaged live. Orthogonal projections were generated and the center images presented are optical sections set at a similar depth of the nucleus (NucBlue staining, white, right panel), as determined by position within the Z-stack. Scale bars in all panels = 20 μm.

3.4. Summary

TaT$_{47-57}$ sequence (RKKRRQRRR) has been shown to internalize into several cell types with different cargos. The downside with TaT-sequence internalization is that only 1% of cargos actually reach their destination because they are trapped in the endosomes. In the past, cargos have escaped the endosomes with the help of peptides such as the pH-dependent membrane active peptides *(112)*. Hypothesizing that intracellular calcium levels would affect calmodulin target proteins, we designed a new CPP-adaptor using the penetrating TaT sequence conjugated with CaM, TaT-CaM, having a His-tag on the N-terminus for purification. We also designed several prototype calmodulin binding cargos: CBS-β-gal, CBS-HRP, and CBS-Myo.

Binding kinetics of TaT-CaM-CBS-proteins interaction was obtained using an optical biosensor. The kinetics of all three protypes was indistinguishable from that obtained between wild type CaM and eNOS. CBS-cargo proteins bound TaT-CaM through BLI analysis with sub-nanomolar concentration resulting in a quick on and slow off rate including the dissociation in EDTA.

Cell penetration assay with confocal laser scanning microscopy analysis showed uniform distribution of CBS-Myo, CBS-HRP, and CBS-β-gal in the cytoplasm of BHK 21, HEK 298T and HT-3 cells *(113)*. This is an indication that the cargos were not trapped in the endosomes. Therefore, the prototype, TaT-CaM was able to translocate cargo proteins of different sizes, overcome the endosomal problem and delivered the cargo proteins in the cytoplasm of living cells. Therefore, this technology has the potential to deliver cargos to different organelles given the appropriate localization signal.

4. UPTAKE KINETICS, DOSAGE CONCENTRATION, CYTOTOXICITY AND SUBCELLULAR LOCALIZATION OF CPP-ADAPTORS/CARGOS

4.1. Uptake Kinetics

Kinetics studies of CPPs are an important tool for understanding the uptake process of cargos. Kinetics explains the rate at which cells take up CPPs and the maximum quantity taken in can be predicted. Kinetics studies are also essential since they could provide important ways to elucidate the mechanism by which CPPs go through the membranes and get into cells. These kinetics measurements can be performed as single time points or as a function of time.

Single Time Point Measurement: A single time point experiment is one way to measure the kinetics of CPP internalization in which the amount of internalized CPP is measured at only one time point. This has the benefit of speed and only a small amount of used material is lost, however it does not provide kinetic constants thereby limiting the information derived *(114)*.

Kinetics Measurements as a Function of Time: The amount of internalized CPP is better obtained as a function of time. Reliable results are obtained when the kinetic data is collected over a long period of time. At long time intervals, the amount of internalized CPPs approach equilibrium with that in the surrounding solution. Because the mechanism of internalization of CPPs is not well known, any kinetic data is either phenomenological or model based *(114)*.

For this reason, first-order kinetics is used as a first approximation and the kinetic

parameters are obtained by fitting in the equation the experimental points:

$$[A] = [A]_\infty \ (1 - e^{-kt})$$

Where [A] is the concentration of internalized CPP at time point t, $[A]_\infty$ is the final

concentration of CPP inside the cells, and k is the first-order rate constant. Goodness of

fit should be tested the entire time interval of the progress curve and analysis of residuals

should be conducted to detect possible trends in discrepancy between the calculated curve

and the experiment points. If goodness of fit is not satisfactory, then other equations need

to be applied, typically involving more complex internalization mechanisms *(114)*.

We examined the uptake kinetics of TaT-CaM- CBS-Myo complex in BHK cells

and S2 cells at one fixed concentration at different times. The two techniques used for

this analysis were confocal laser scanning microscopy as described in chapter 3 and flow

cytometry, FACs (Fluorescence Activating Cell sorting). Flow cytometry is an important

method of counting, examining and sorting cells in suspension. It allows for the

characterization of physical or chemical attributes of cells as they flow through an optical

detector. Based on this analysis, flow cytometry is able to distinguish a population of

cells based on size, viability, protein expression, fluorescently labelled proteins and

several other features. Here flow cytometry was used to monitor how fast TaT-CaM and

CBS-Myo were taken up by BHK and S2 cells.

4.1.1　Method

Exponentially growing BHK 21 cells were incubated with cell tracker for 20min then NucBlue for 10min prior to treatment. Z-Stack positions were set with the cells. The cells were treated with TaT-CaM and CBS-Myo to a final concentration of 100nM and images recorded over an hour at 5min intervals. As shown in Figure 19 below, it was difficult to get real time kinetics for the 1hr time period because penetration was observed within the first 5min of treatment. We next attempted uptake kinetic studies using the flow cytometer, BHK cells were trypsinized to lift them up. No kinetics data was recorded with BHK on the flow because, no penetration was observed. This might be explained by a key difference in the procedure, trypsinizing the cells may impact the import machinery found on cell surfaces. We then turned to examine cells already in suspension in this case S2 cells.

S2 insect cells from *Drosophila melanogaster* embryos growing at room temperature at ambient CO_2 were used for CPP-adaptor kinetic studies. This is necessary because trypsinizing adherent cells appears to import machinery of cargos. Untreated cells were used to set the baseline and gates for the experiment. The cells were treated with TaT-CaM and CBS-Myo to a final concentration of 500nM

4.1.2.　Results and Discussion

FACS analysis is a conventional tool to quantify cellular association of fluorochrome-tagged peptides. However, flow cytometry does not discriminate between membrane-bound and internalized fluorescently labelled cargos, thus limiting the use of this technique. This limitation is observed with the data in figure 19A with the control at different incubation periods being similar to the experimental.

Examination of the time course of TaT-CaM conjugated CBS-Myo uptake using confocal microscopy showed localization of the CBS-Myo in the cytoplasm within 5mins (Figure 19 B). Z-stack analysis showed that after five minute, fluorescence becomes constant. The rapid internalization of the cargos by TaT-CaM suggests that clatherin-mediated endocytosis is the mode of entry. Other experiments will be performed to test this idea.
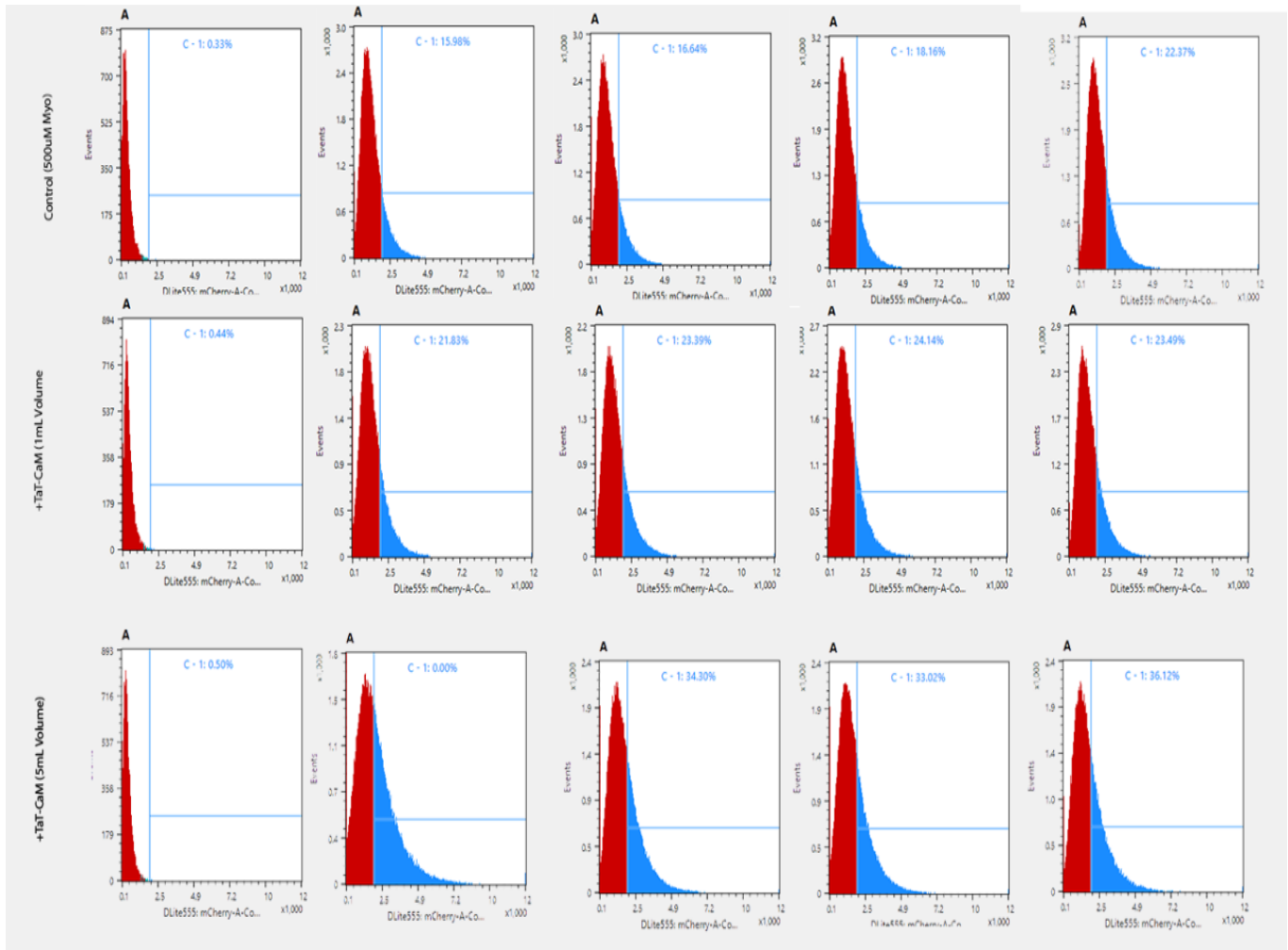
Figure 19A. Using FACScan to determine the kinetics of CBS-Myo delivery by TaT-CaM. The population of S2 cells was gated base on the Forward Scatter (FSC) and side scatter (SSC). From left to right shows the untreated cells and then treated cells at different time points. The top row represents CBS-Myo (500nM) control only. The middle row represents cells treated with TaT-CaM(500nM) and CBS-Myo (500nM) in 1ml final volume and the last row is cells treated in 5ml final volume. Each column represents untreat cells, treatment for 5min, 10min, 20min and 30min respectively
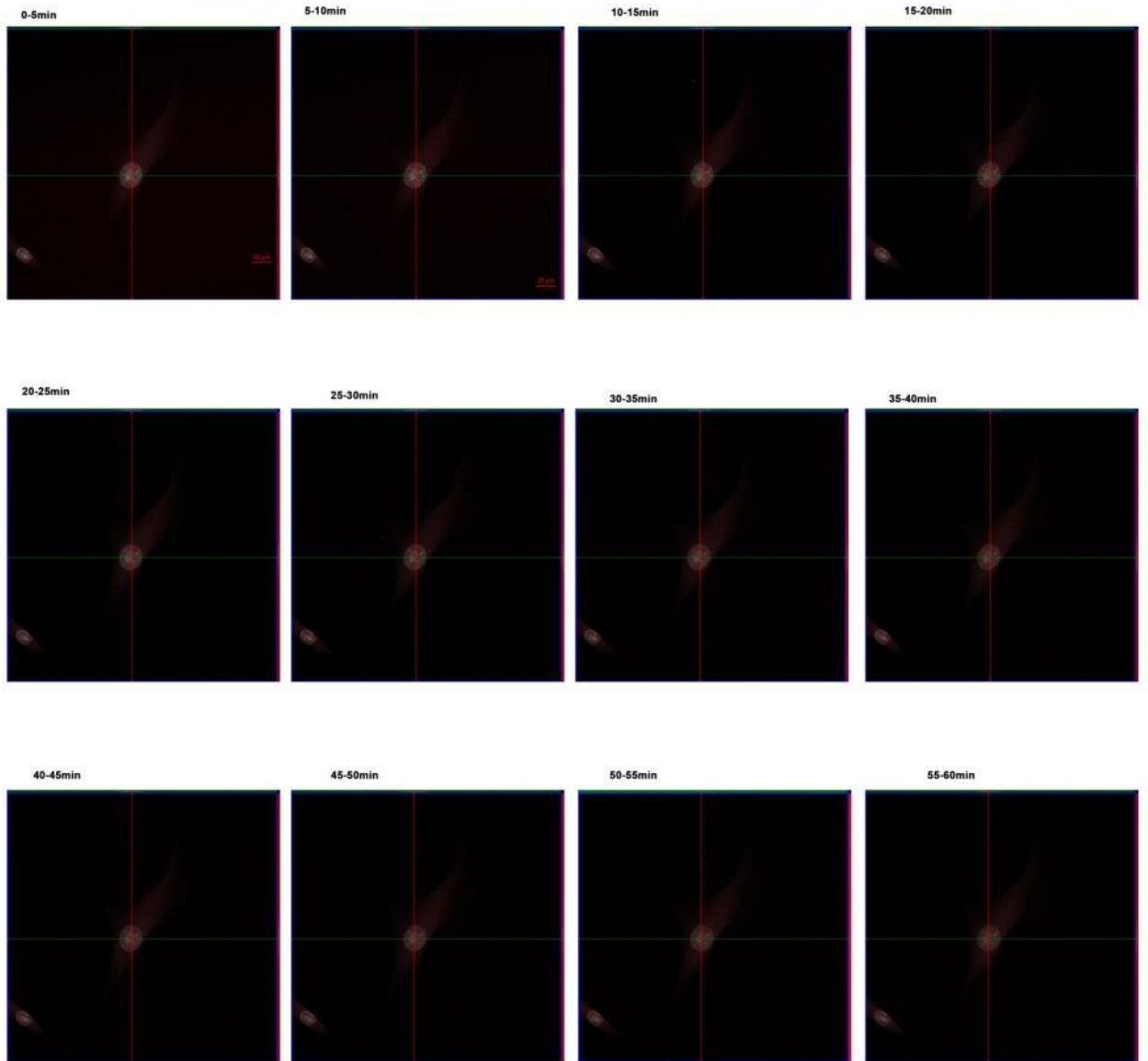
Figure 19B: Using confocal microscopy to determine the kinetics of CBS-Myo delivery by TaT-CaM. BHK cells were stained with cell tracker followed by NucBlue. Z-stack positions were established and then cells were treated with the TaT-CaM-CBS-Myo complex (100nM). Images were obtained over 1hr at 5mins interval. In summary, no significant change is observed after 5mins of treatment.

4.2. Dose Concentration and Cytotoxicity

4.2.1. Dose concentration

We initially used 1μM final concentration of both TaT-CaM and cargos to test penetration. To find out the minimum dose that is effective, we tested 3 different concentrations 1nM, 100nM and 500nM. Confocal images showed penetration with all three concentrations Figure 20.

4.2.2. Cytotoxicity

High concentrations of TaT peptide initiate apoptosis in endothelial cells (112). For TaT-CaM to be used as a therapeutic delivery tool, it must be well tolerated; we analyzed higher concentrations of TaT-CaM to determine the impact on cellular health. BHK cells were treated as in Figure 21 and pictures were taken 48h after incubation with the indicated concentrations. For all concentrations, there was no change in morphology with the BHK cells. This implies that TaT-CaM is not toxic to cells even at a 50 fold increase from our standard concentration of 1μM (*(113)*.
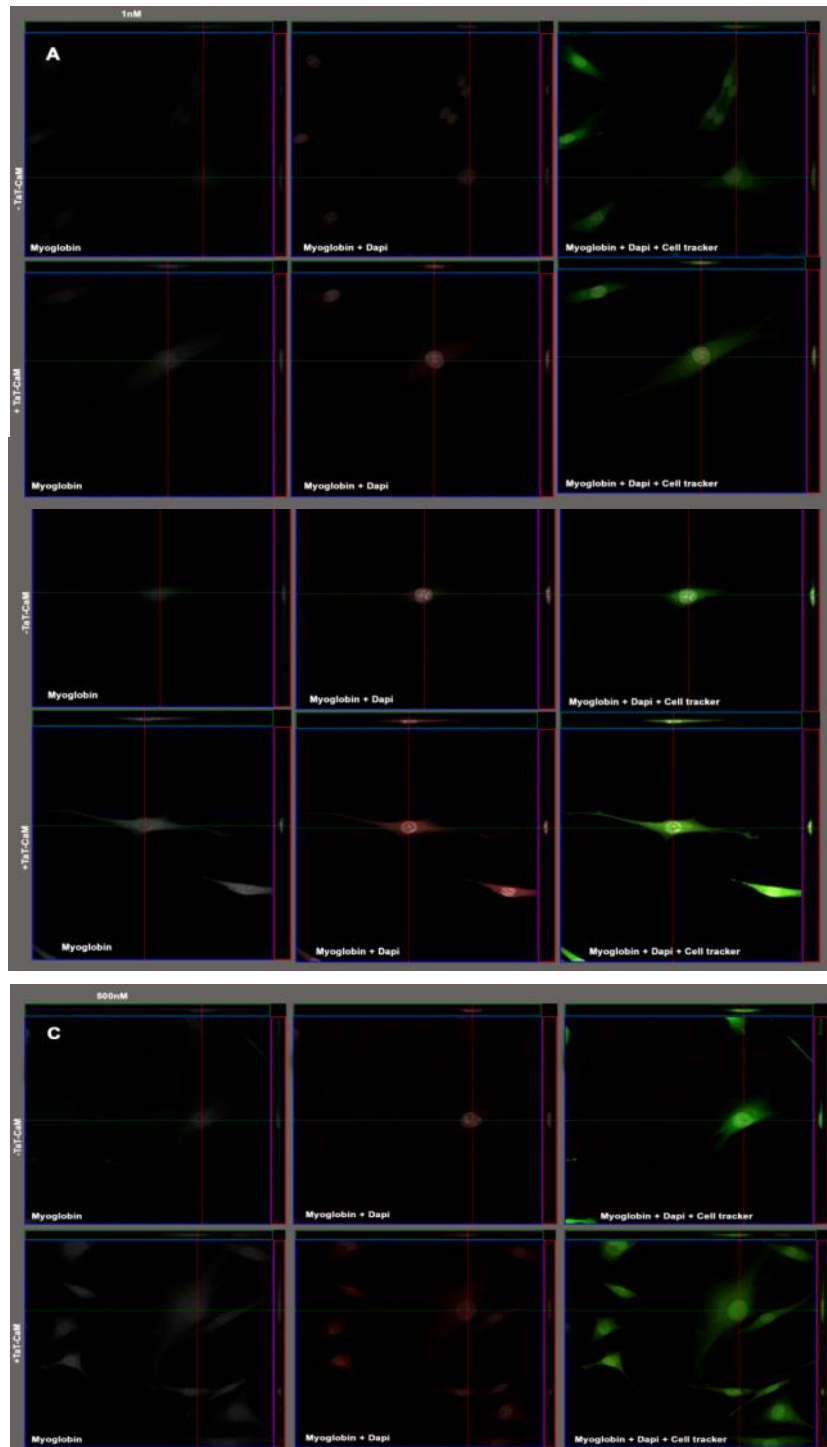
Figure 20: Dose concentration showing three different TaT-CaM and CBS-Myo **(A) 1nM, (B) 100nM, (C) 500nM** concentrations. BHK cells were treated with various concentrations of CBS-Myo with or without TaT-CaM for 15mins. Cells were washed 3x with PBS followed by incubation in 2uM cell tracker green dye for 20min. Washed 3x then Nucblue staining for 10min. Imaged in 25mM HEPES pH 7.4 medium.
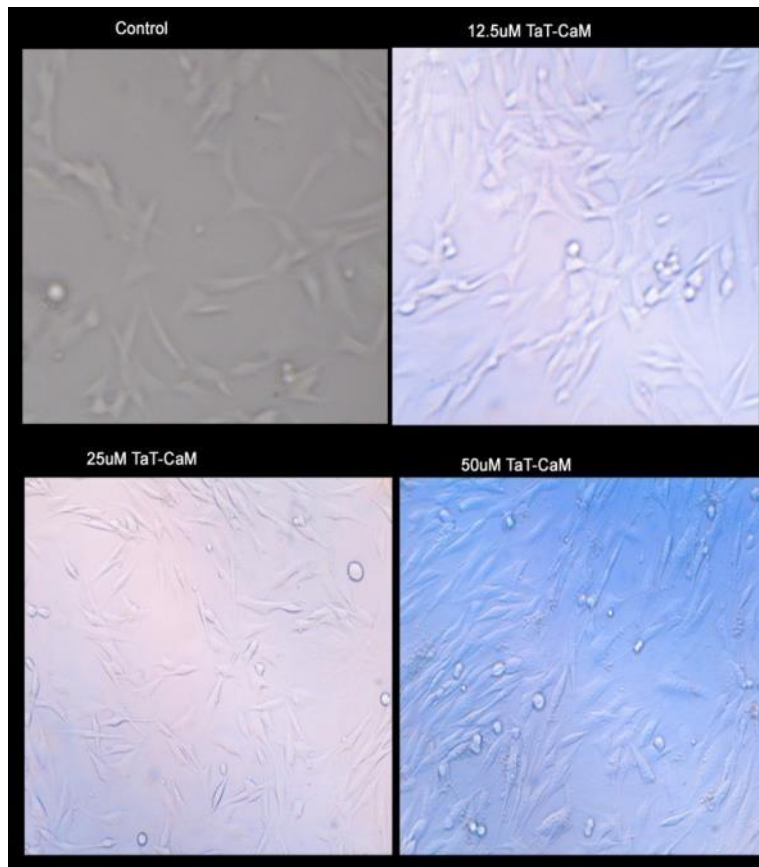
Figure 21: Dose concentration of TaT-CaM checking for cytoxicity. BHK cells were treated with various TaT-CaM concentrations as listed on the images and pictures were taken after 48h. No significant changes in morphology were noted.

4.3. Subcellular localization of TaT-CaM and CBS-cargos in the Nucleus and Endoplasmic Reticulum

Subcellular localization signals determine the environments in which eukaryotic proteins reside. Subcellular localization influences protein function by controlling access to and availability of all types of molecular interaction partners. Therefore, knowledge of protein localization often plays a significant role in characterizing the cellular function of hypothetical and newly discovered proteins. Subcellular location of a protein can be determined either by mass spectrometry (where cellular organelles are analyzed for protein composition) *(115)* or by protein labeling. The latter is then analyzed by fluorescence microscopy.

The nucleus is the major cellular component where transcription of genes take place, and it is the major target for drugs. However, transport of therapeutic molecules from cytoplasm to the nucleus remains a challenge. Studies on the nuclear pore complex have enabled CPPs to be designed with nuclear import signal sequences. These sequences, nuclear localization sequences (NLSs), are characterized by short sequences with at least one or two clusters of four or more basic amino acids *(116)*. The most common sequence used is the monopartite NLS, PKKKRKV, derived from simian virus 40 (SV40) large T antigen. This NLS has been used to couple cargoes such as proteins, peptides and DNA, allowing these coupled proteins to cross the nuclear membrane *(116)*.

The endoplasmic reticulum (ER) is the organelle in eukaryotic cells where proteins are folded. Synthesized proteins are transported in vesicles to the Golgi apparatus and other organelles. Most lipids that are used for the membranes of the

mitochondria and peroxisomes are also synthesized in the ER. Signal sequences were first used to direct the polypeptide chain emerging from ribosomes to a translocator on the ER membrane. Forming a pore in the membrane, the polypeptide was able to translocate into the lumen of the ER *(117)*. This signal sequence also helps to ensure that proteins exported from the cell or those being delivered to specialized organelles reached the ER lumen. With the ER signal sequence, KDEL, attached to any cargo protein, the protein is retained to the ER. Proteins with this sequence will only leave the ER after the sequence has been cleaved off by signal peptidases *(117)*

To test subcellular localization, we designed CBS-Myo with NLS and KDEL sequences. We designed CBS-Myo-NLS and CBS-Myo- KDEL with the idea that if these localization signals are successful, then proteins will be able to be delivered into these organelles using TaT-CaM.

Cell penetration assay with TaT-CaM

 Sub-localization analysis of TaT-CaM was performed by fluorescently labelling TaT-CaM protein with Dylight 550 according to the manufacturer's protocol and as described in chapter 3. BHK cells were treated with 100nM labeled TaT-CaM for 15min. The cells were washed three times with PBS containing calcium and magnesium. Localization was observed with confocal microscopy. Using cell tracker dye (green) to stain the cytoplasm and NucBlue for the nucleus, we were able to identify TaT-CaM in the endosomes (Figure 22).

These results were confirmed with fixed cells. Briefly, BHK cells were treated with TaT-CaM complex with CBS-Myo. The cells were washed 3 times with PBS then

fixed with 4% PFA + 0.1% Triton-X-100 with rocking at room temperature for 20min.

The cells were blocked with PBS/5% BSA for an hour. The fixed cells were probed

overnight at 40^0C with anti-calmodulin 1:1000 dilution. TaT-CaM localization was

observed using the secondary antibody, goat anti-rabbit Alexa 488 (1:200). The control

for this test was probing for untreated cells with anti- calmodulin testing for endogenous

calmodulin.
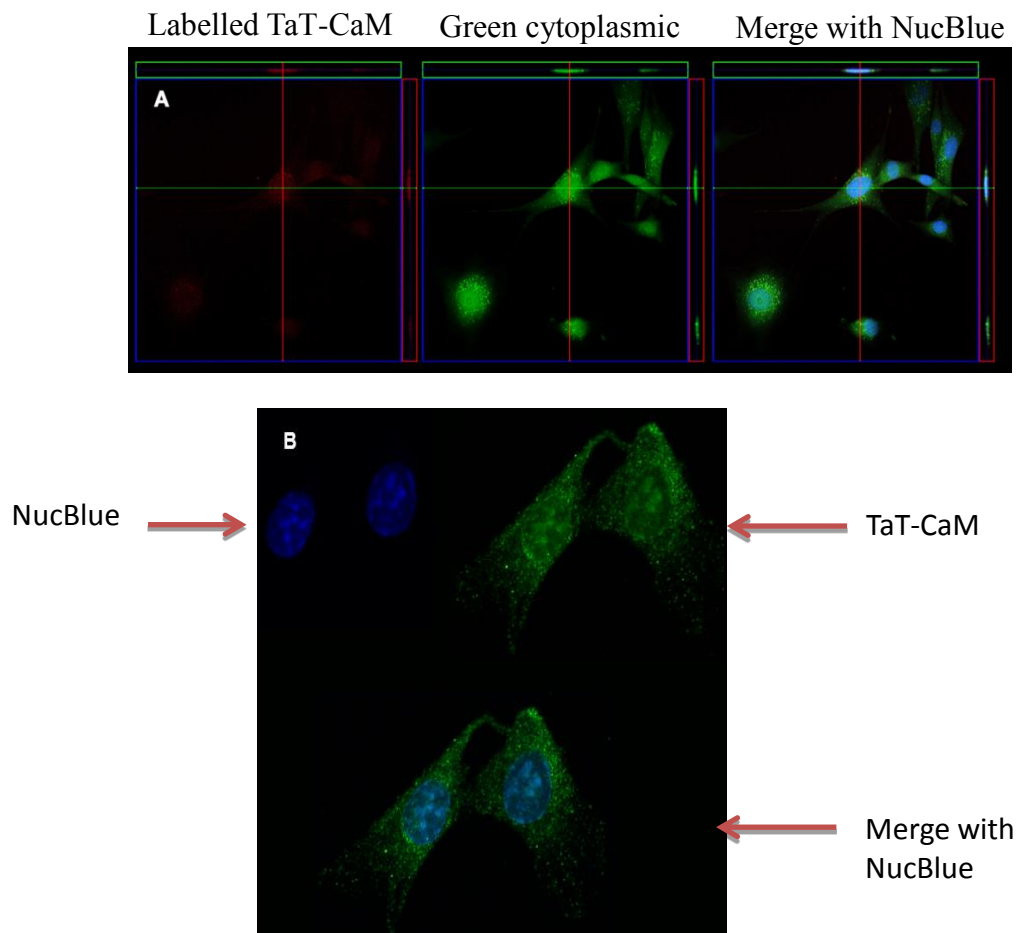
Figure 22: BHK cells were treated with TaT-CaM in live cells **(A)** or fixation **(B)**.
Nucleus and cytoplasm were stained with NucBlue and cell-tracker green dye
respectively. A) Live cells treated with labeled TaT-CaM (red) for 15mins. B) Cells
after incubation with TaT-CaM were fixed in 4% PFA for 20mins then blocked in
PBS/5% BSA + 0.1% Triton-X-100.

Cell penetration Assay with CBS-Myo-NLS

BHK cells were treated for 20 minutes with CellTracker Green CMFDA dye
(rendered as green) followed by two PBS/Ca^{2+}washes. They were again treated for 10
minutes with NucBlue (rendered as blue).The cells were treated with 100nM of Dylight
550 fluorescently labeled cargo protein CBS-Myoglobin-NLS (rendered as red) in buffer
containing 1 mM CaCl$_2$, either in the presence or absence of 100nM TaT-CaM for 30min.
Afterwards the cells were washed and imaged by fluorescence confocal microscopy. Z-
stacks were set using the NucBlue staining of the nucleus as a reference. Orthogonal
projections of Z-stacks were generated using Zeiss Zen software. As shown in Figure
(Figure 23), CBS-Myo-NLS in the presence of TaT-CaM is entering into the cell, and is
being transported via the nuclear pore complex into the nucleus.
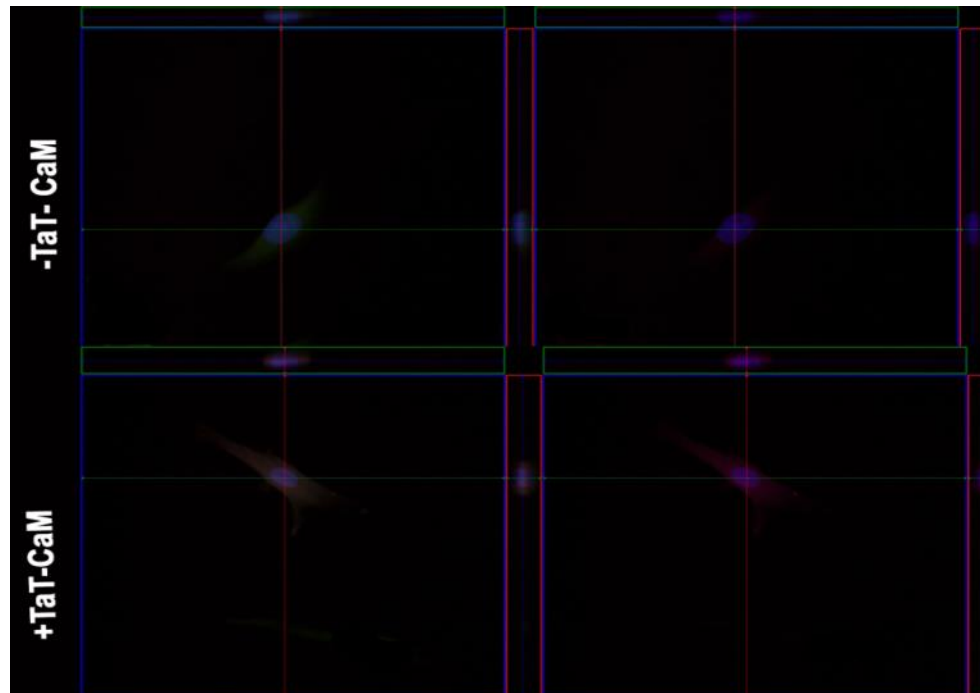
Figure 23: Confocal imaging of cell penetration. BHK cells were treated for 20 minutes with
CellTracker Green CMFDA dye (green in left panels). Then treated for 10 minutes with
NucBlue. Then treated with 100nM DyLight 550 fluorescently labeled cargo protein CBS-
Myo-NLS (rendered as red) in either the absence or presence of 100nM TaT-CaM.

Cell penetration Assay with CBS-Myo-KDEL

BHK cells were treated for 20 minutes with CellTracker DEeep Red dye (rendered as magenta). The cells were then treated for 20 minutes with ER dye (rendered as green) followed by a 10 minutes NucBlue treatment (rendered as white). The cells were then treated with 100nM of Dylight 550 fluorescently labeled cargo protein CBS-Myo-KDEL (rendered as red) in buffer containing 1 mM $CaCl_2$, either in the presence or absence of 100nM TaT-CaM for 30min. Afterwards the cells were washed and imaged by fluorescence confocal microscopy. Z-stacks were set using the NucBlue staining of the nucleus as a reference. Orthogonal projections of Z-stacks were generated using Zeiss Zen software. As shown in Figure 24, CBS-Myo-KDEL in the presence of TaT-CaM is entering into the cell, and is localizing in the ER.
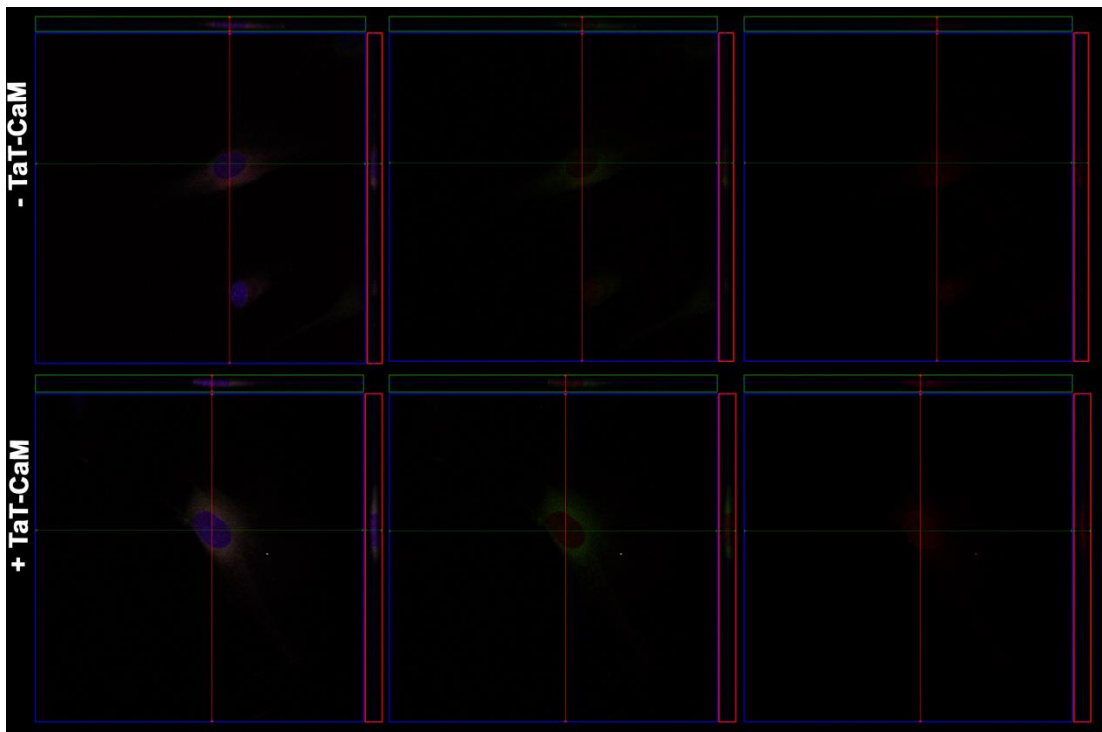
Figure 24. Confocal imaging of cell penetration. BHK cells were treated for 20 minutes with CellTracker Deep red dye (magenta in left panels) followed ER dye for 20min (green). Then, treated for 10min with NucBlue. Cells were treated with 100nM DyLight 550 fluorescently labeled CBS-Myo-KDEL(red), in either the absence or presence of 100nM TaT-CaM for 15 min.

4.4.   Summary

We attempted to examine the uptake kinetics of TaT-CaM with cargo complex by BHK cells. With confocal microscopy, after the first 5min, the results did not change upon TaT-CaM/CBS-Myo addition. This suggests that penetration occurs within 5min of TaT-CaM treatment. Attempting to visualize uptake faster using flow cytometry, trypsinized BHK cells were used to flow on the FACs, but no penetration was observed. We think that trysin impacts the cell uptake machineries. Using insect cells growing in suspension, it was difficult to analyze uptake versus surrounding since controls looked just like experimentals. A re-evaluation is required on how to evaluate uptake kinetics. A possibility is using a microfluidics chamber on the confocal microscope and imaging cells during treatment.

We also performed both labeling and immunohistochemistry to identify the location of TaT-CaM when it let go of cargos in the cell. The data suggests TaT-CaM location to be in the endosomes. Using the nuclear and the ER subcellular localization sequences, preliminary studies showed that CBS-Myo-NLS and CBS-Myo-KDEl in the presence of TaT-CaM were transported into the nucleus and ER respectively.

5. APPLICATIONS OF CPP-ADAPTORS AND FUTURE DIRECTIONS

As stated, one of the aims of this project was to design new cell penetrating peptide-adaptors that would be used for the internalization of biological molecules. Macromolecular compounds, like proteins, oligonucleotides and polypeptides consist of capabilities and therapeutic features that are highly sought after. However, large macromolecule intracellular delivery *in vivo* has not been realized because they have low to no bioavailability and require delivery vehicles. Even though multiple classes of delivery vehicles have been developed and significant progress has been made, there are still inadequate robust and safe uptake formulations. The ability of CPPs to translocate rapidly into cells is being exploited and this technique has led to the delivery of a broad range of therapeutics including proteins, DNA, antibodies, oligonucleotides, imaging agents and liposomes in a variety of situations and biological systems. Previous CPPs have shown great potential and have even been used in the treatment of human diseases such as neuronal disease, asthma, ischemia, diabetes, and cancer *(113)* however inefficient endosomal escape has remained a major challenge. Our CPP-adaptor has overcome this challenge unleashing an unlimited number of possibilities and applications.

Covalently linked small molecules to CPPs have shown proof of concept of optimal delivery. However, attaching CPPs to small molecules may not be the best method for the delivery of all types of therapeutic molecules. Covalent coupling to a peptide could interfere with the function of biologically active molecules, for example oligonucleotides and proteins, possibly by causing steric hindrance of drug binding to targets. Therefore, for macromolecule cargoes, non-covalent CPP complexes might provide a better drug delivery solution.

Protein delivery by CPPS

Proteins and peptides have significant potential as theraputics for the treatment of various human diseases including storage diseases and cancer. Storage diseases are those that are caused by the deficiency of certain enzymes especially lysosomal enzymes *(118)* and they can be treated only by administering exogenous enzymes. These enzymes and other proteins have been coupled to CPPs for delivery. CPPs deliver proteins ranging in size from 30kDa (GFP) to 150KDa (IgG). Therapeutic relevant proteins have been delivered by CPPs and they have significant potential in cancer and stroke treatment *(119)*.

Drug delivery by CPPs in cancer cells

One relevant clinical application of CPPs is the delivery of drug for conventional cancer chemotherapeutics as well as oligonucleotide based treatments. Due to CPPs ability to transport cargos through the cellular plasma membrane, a large number of different drug-CPP constructs have been synthesized. The cargos, that have been delivered, range from classical molecular drugs to different types of oligonucleotides and

proteins. For example, in cancer chemotherapy, toxic drugs are conjugated to CPPs and delivered more efficiently than previous drug administration methods *(120)*.

TaT, penetratin, and several other CPPs have been use to deliver chemotherapy drugs into tumor cells. One such example is doxorubicin (DOX), a drug commonly used to treat various types of cancers. Even though DOX has been used to treat many different cancers, it has difficulty crossing the blood brain barrier. This brain barrier challenge is due to the tight endothelial cell junctions at the blood brain barrier. Coupling DOX to CPPs, the uptake was 20 fold higher into the brain parenchyma than free DOX *(121)*. Another anticancer agent, Methotrexate (MTX) which is not frequently used due to tumor cell resistance, was delivered into tumor cells using the CPP YTA2 *(122)*. MTX-CPP was successfully delivered into tumor cells, hence overcoming MTX resistance in the breast cancer cell line MDA-MB-321, thereby restoring the effect of MTX and rendering the tumor cells once again sensitive for chemotherapy *(122)*.

Delivery of Macromolecules by CPPs for tumor targeting

CPPs used in gene therapy are able to condense DNA tightly into a small compact particle. The particle should be able to target the condensate to specific cell surface receptors and finally be able to escape the endosomal trap and target the DNA cargo into the nucleus for gene expression *(29)*. TaT has been fused at the N-terminal domain of the tumor suppressor protein p53 leading to accumulation of p53 in cells and the activation of apoptotic genes. TaT coupled to an anti-p21 antibody was used to block p21 from translocating into nucleus thereby making cancer cells more sensitive to chemotherapy hence reducing the dosage of chemotherapy used *(29)*. Using CPPs to

deliver antibodies directly into the cytoplasm and nucleus of cancer cells has incredible

potential, allowing for the intracellular targeting of cancer-specific protein mutations.

Delivery of imaging agents

The ability to visualize internal features of living organisms and observe cellular

functions *in vivo* has the potential to improve disease management by detecting disease

markers, diagnosing, and treating diseases. Imaging technologies also make it easy to

detect the stage of diseases, identify the extent of disease and measure the effect of

treatment. Magnetic resonance imaging (MRI) is the most used imaging technique on soft

tissue. Images are obtained based on nuclei exposure to a static magnetic field. Other

imaging agents are required to image angiogenesis, and apoptosis, but again permeability

of these imaging agents remains a challenge. CPPs again have been used in this field to

deliver imaging agents, contrast agents and quantum dots (QDs) *(1)*.

We designed optimized and developed TaT-CaM and Ant-CaM. Fluorescently

labeled calmodulin binding site proteins: CBS-Myo, CBS-HRP, CBS-β-gal were

delivered into eukaryotic cells (BHK, HEK 293T, HT3). Because endosomal entrapment

has been a significant problem for CPP delivery, we analyzed cargo delivery with an

inverted confocal microscope and were able to detect the cargos in the cytoplasm of the

cells. Further analysis revealed that after delivery of cargos, TaT-CaM was entrapped in

the endosomes. This indicates selective delivery of cargos and that after TaT-CaM has

completed its function it will be broken down and removed from the cell. The work

described so far was achieved using micromolar concentrations. This represents an

optimal concentration between the CPP-adaptor and the cargos giving the CPP-adaptor

the ability to promote endosomal escape and deliver cargoes at higher rates. This is significant because a lower concentration of drugs can be used when an optimal CPP-adaptor is used therefore, reducing toxicities and side effects.

CPPs applications are widely used as drug delivery tools because they are low in cytotoxicity. Comparative cytotoxicity studies between the basic (TaT and penetratin) and amphipathic peptides (transpotan and MAP) showed that amphipathic peptides have been associated with membrane leakage *(114)*. These analyses using lactate dehydrogenase confirmed that transportan and MAP were involved in membrane leakage that was associated with the hydrophobic residues in these peptides. On the other hand, basic peptides were mild in toxicity.

Another application of CPPs in cancer treatment involves small anticancer drugs being able to diffuse into cancer cells directly. The only issue with this is that after repeated exposure of the same drug a tumor cell could develop multidrug resistance *(115)*. CPP-adaptors would be very promising in this area since they are able to deliver both small and large molecules. By delivering a mixture of both small and large molecules the CPP could postpone the development of multidrug resistance in tumor cells. CPPs have also been used to improve internalization across the blood barrier of the brain *(116)*. Considering the work, we showed with subcellular localization, our CPP-adaptors are eligible to internalize any cargo into a specific organ or tissue as long as it has the localization signal.

Future directions

The first objective of this study was achieved. Moving forward, we would alter the environment of a cell by using the CPP-adaptor to penetrate an active kinase in the cell. Numerous diseases are associated with stress responses. The cellular stress response includes unfolded or misfolded protein accumulation and organelle deterioration. Thus, enhanced activation of pathways that have evolved to protect against these defects may protect against degenerative diseases such as Parkinson's and Alzheimer's *(123)*. Generally, stress response pathways are maintained in the off state or at a baseline level. The perturbation of an organelle or stimulation from external stimuli would activate these pathways. Once activated, they stayed on to efficiently promote cellular survival and organelle recovery. When the stimuli are removed, the pathways are regulated so that cells can properly respond to future stress. For example, the p38 MAPK pathway also known as p38 SAPK (Stress Activated Protein Kinase) protein kinase is activated by different stress stimuli. p38 plays a key role in the regulation of cellular responses to many types of stresses, and also in the regulation of proliferation, differentiation, survival and development of specific cell types *(124-126)*.

The JNK pathways are another example of a stress activating pathway. JNK activities strongly increase in response to different stresses such as cytokines, UV irradiation, growth factor deprivation, and agents that interfere with DNA and protein synthesis *(126)*. JNKs are also involved in stress-induced and developmentally programmed apoptosis as well as cell transformation *(126)*. Examining the cytotoxicity of CPPs, TaT-peptide and antennapedia results showed that at higher concentrations, stress

response pathways, JNK and p38 are activated with JNK being more severe than p38 *(127)*. Treating cells with TaT-CaM and finding out if stress response pathways are turned on will be an interesting finding. Our toxicity results of BHK cells treated with 50μM TaT-CaM showed no morphology change after 48hrs. We will analyze these stress pathways by treating the cells with TaT-CaM and probing the cell lysates to determine the activities of p38 and /or JNK kinases. Also, we will shuttle an active p38 or JNK kinase into cells and monitor activity.

This work has demonstrated the feasibility of delivery of a variety of cargo proteins and has opened up an array of potential research in diagnostic and therapeutic applications. Another area of investigation includes the mechanism of internalization. Knowing that TaT-CaM delivery cargos escaped endosomal trap, it would be important to understand if the TaT-CaM/ CBS-proteins are fully enveloped in the endosomes or it is sitting on the endosomal membrane with TaT-CaM in the vesicle and CBS-proteins outside. This can be achieved by organelle isolation. Endosomes can be extracted and treated in the presence and absence of proteinase K. If it is in the vesicle, then more will be observed in the plus proteinase K treated. But if it is outside, then more will be seen in the negative proteinase K treated.

References

1. Farkhani, S. M.; Valizadeh, A.; Karami, H.; Mohammadi, S.; Sohrabi, N.; Badrzadeh, F. Cell penetrating peptides: Efficient vectors for delivery of nanoparticles, nanocarriers, therapeutic and diagnostic molecules. *Peptides* **2014***, 57*, 78-94.

2. Vives, E.; Brodin, P.; Lebleu, B. A truncated HIV-1 Tat protein basic domain rapidly translocates through the plasma membrane and accumulates in the cell nucleus. *J. Biol. Chem.* **1997***, 272*, 16010-16017.

3. Lee, S. H.; Castagner, B.; Leroux, J. Is there a future for cell-penetrating peptides in oligonucleotide delivery? *European Journal of Pharmaceutics and Biopharmaceutics* **2013***, 85*, 5-11.

4. Torchilin, V. P.; Omelyanenko, V. G.; Papisov, M. I.; Bogdanov, A. A.,Jr; Trubetskoy, V. S.; Herron, J. N.; Gentry, C. A. Poly(ethylene glycol) on the liposome surface: on the mechanism of polymer-coated liposome longevity. *Biochim. Biophys. Acta* **1994***, 1195*, 11-20.

5. Koren, E.; Torchilin, V. P. Cell-penetrating peptides: breaking through to the other side. *Trends Mol. Med.* **2012***, 18*, 385-393.

6. Copolovici, D. M.; Langel, K.; Eriste, E.; Langel, Ü Cell-penetrating peptides: design, synthesis, and applications. *ACS Nano* **2014***, 8*, 1972-1994.

7. Woods, N. B.; Muessig, A.; Schmidt, M.; Flygare, J.; Olsson, K.; Salmon, P.; Trono, D.; von Kalle, C.; Karlsson, S. Lentiviral vector transduction of NOD/SCID repopulating cells results in multiple vector integrations per transduced cell: risk of insertional mutagenesis. *Blood* **2003***, 101*, 1284-1289.

8. Romani, B.; Engelbrecht, S.; Glashoff, R. H. Functions of Tat: the versatile protein of human immunodeficiency virus type 1. *J. Gen. Virol.* **2010***, 91*, 1-12.

9. Sodhi, A.; Montaner, S.; Gutkind, J. S. Viral hijacking of G-protein-coupled-receptor signalling networks. *Nature Reviews Molecular Cell Biology* **2004***, 5*, 998.

10. Flávia Helena, d. S.; Tiago, P. D.; Nance, B. N. Beyond retrovirus infection: HIV meets gene therapy. *Genetics and Molecular Biology* **2006**, 367.

11. Bechara, C.; Sagan, S. Cell-penetrating peptides: 20 years later, where do we stand? *FEBS Lett.* **2013***, 587*, 1693-1702.

12. Green, M.; Loewenstein, P. M. Autonomous functional domains of chemically synthesized human immunodeficiency virus tat trans-activator protein. *Cell* **1988***, 55*, 1179-1188.

13. Frankel, A. D.; Pabo, C. O. Cellular uptake of the tat protein from human immunodeficiency virus. *Cell* **1988***, 55*, 1189-1193.

14. Derossi, D.; Joliot, A. H.; Chassaing, G.; Prochiantz, A. The third helix of the Antennapedia homeodomain translocates through biological membranes. *J. Biol. Chem.* **1994***, 269*, 10444-10450.

15. Derossi, D.; Chassaing, G.; Prochiantz, A. Trojan peptides: the penetratin system for intracellular delivery. *Trends Cell Biol.* **1998***, 8*, 84-87.

16. Thorén, P. E. G.; Persson, D.; Karlsson, M.; Nordén, B. The Antennapedia peptide penetratin translocates across lipid bilayers – the first direct observation. *FEBS Lett.* **2000***, 482*, 265-268.

17. Elmquist, A.; Lindgren, M.; Bartfai, T.; Langel, Ü VE-Cadherin-Derived Cell-Penetrating Peptide, pVEC, with Carrier Functions. *Exp. Cell Res.* **2001***, 269*, 237-244.

18. Kobayashi, S.; Takeshima, K.; Park, C. B.; Kim, S. C.; Matsuzaki, K. Interactions of the novel antimicrobial peptide buforin 2 with lipid bilayers: proline as a translocation promoting factor. *Biochemistry* **2000***, 39*, 8648-8654.

19. Aints, A.; Guven, H.; Gahrton, G.; Smith, C. I.; Dilber, M. S. Mapping of herpes simplex virus-1 VP22 functional domains for inter- and subcellular protein targeting. *Gene Ther.* **2001***, 8*, 1051-1056.

20. Elliott, G.; O'Hare, P. Intercellular Trafficking and Protein Delivery by a Herpesvirus Structural Protein. *Cell* **1997***, 88*, 223-233.

21. Phelan, A.; Elliott, G.; O'Hare, P. Intercellular delivery of functional p53 by the herpesvirus protein VP22. *Nat. Biotechnol.* **1998***, 16*, 440-443.

22. Schmidt, N.; Mishra, A.; Lai, G. H.; Wong, G. C. Arginine-rich cell-penetrating peptides. *FEBS Lett.* **2010***, 584*, 1806-1813.

23. Futaki, S.; Suzuki, T.; Ohashi, W.; Yagami, T.; Tanaka, S.; Ueda, K.; Sugiura, Y. Arginine-rich peptides. An abundant source of membrane-permeable peptides having potential as carriers for intracellular protein delivery. *J. Biol. Chem.* **2001***, 276*, 5836-5840.

24. Oehlke, J.; Scheller, A.; Wiesner, B.; Krause, E.; Beyermann, M.; Klauschenz, E.; Melzig, M.; Bienert, M. Cellular uptake of an α-helical amphipathic model peptide with the potential to deliver polar compounds into the cell interior non-endocytically. *Biochimica et Biophysica Acta (BBA) - Biomembranes* **1998***, 1414*, 127-139.

25. Pooga, M.; Hallbrink, M.; Zorko, M.; Langel, U. Cell penetration by transportan. *FASEB J.* **1998**, *12*, 67-77.

26. Wang, F.; Wang, Y.; Zhang, X.; Zhang, W.; Guo, S.; Jin, F. Recent progress of cell-penetrating peptides as new carriers for intracellular cargo delivery. *J. Controlled Release* **2014**, *174*, 126-136.

27. El-Sayed, A.; Futaki, S.; Harashima, H. Delivery of macromolecules using arginine-rich cell-penetrating peptides: ways to overcome endosomal entrapment. *AAPS J.* **2009**, *11*, 13-22.

28. Jo, J.; Hong, S.; Choi, W. Y.; Lee, D. R. Cell-penetrating peptide (CPP)-conjugated proteins is an efficient tool for manipulation of human mesenchymal stromal cells. *Sci. Rep.* **2014**, *4*.

29. Bolhassani, A. Potential efficacy of cell-penetrating peptides for nucleic acid and drug delivery in cancer. *Biochimica et Biophysica Acta (BBA) - Reviews on Cancer* **2011**, *1816*, 232-246.

30. Rizzuti, M.; Nizzardo, M.; Zanetta, C.; Ramirez, A.; Corti, S. Therapeutic applications of the cell-penetrating HIV-1 Tat peptide. *Drug Discov. Today* **2015**, *20*, 76-85.

31. Carter, J.; Saunders, V. *Virology: Principles and Applications*. John Wiley and Son, Ltd: England, 2007, pp 198-207.

32. Richman, D. D.; Margolis, D. M.; Delaney, M.; Greene, W. C.; Hazuda, D.; Pomerantz, R. J. The challenge of finding a cure for HIV infection. *Science* **2009**, *323*, 1304-1307.

33. Yang, Y.; Ma, J.; Song, Z.; Wu, M. HIV-1 TAT-mediated protein transduction and subcellular localization using novel expression vectors. *FEBS Lett.* **2002**, *532*, 36-44.

34. Wong, K.; Sharma, A.; Awasthi, S.; Matlock, E. F.; Rogers, L.; Van Lint, C.; Skiest, D. J.; Burns, D. K.; Harrod, R. HIV-1 Tat interactions with p300 and PCAF transcriptional coactivators inhibit histone acetylation and neurotrophin signaling through CREB. *J. Biol. Chem.* **2005**, *280*, 9390-9399.

35. Yedavalli, V. S.; Benkirane, M.; Jeang, K. T. Tat and trans-activation-responsive (TAR) RNA-independent induction of HIV-1 long terminal repeat by human and murine cyclin T1 requires Sp1. *J. Biol. Chem.* **2003**, *278*, 6404-6410.

36. Zheng, C. F.; Simcox, T.; Xu, L.; Vaillancourt, P. A new expression vector for high level protein production, one step purification and direct isotopic labeling of calmodulin-binding peptide fusion proteins. *Gene* **1997**, *186*, 55-60.

37. Vives, E.; Brodin, P.; Lebleu, B. A truncated HIV-1 Tat protein basic domain rapidly translocates through the plasma membrane and accumulates in the cell nucleus. *J. Biol. Chem.* **1997**, *272*, 16010-16017.

38. Su, Y.; Doherty, T.; Waring, A. J.; Ruchala, P.; Hong, M. Roles of Arginine and Lysine Residues in the Translocation of a Cell-Penetrating Peptide from (13)C, (31)P and (19)F Solid-State NMR. *Biochemistry (N. Y.)* **2009**, *48*, 4587-4595.

39. Fuchs, S. M.; Raines, R. T. Pathway for Polyarginine Entry into Mammalian Cells. *Biochemistry (N. Y.)* **2004**, *43*, 2438.

40. Loret, E. P.; Georgel, P.; Johnson, W. C.; Ho, P. S. Circular dichroism and molecular modeling yield a structure for the complex of human immunodeficiency virus type 1 trans-activation response RNA and the binding region of Tat, the trans-acting transcriptional activator. *Proc. Natl. Acad. Sci. U. S. A.* **1992**, *89*, 9734-9738.

41. Carroll, S. B.; Laymon, R. A.; McCutcheon, M. A.; Riley, P. D.; Scott, M. P. The localization and regulation of Antennapedia protein expression in Drosophila embryos. *Cell* **1986**, *47*, 113-122.

42. Talbert, P. B.; Garber, R. L. The Drosophila Homeotic Mutation Nasobemia (Antp(ns)) and Its Revertants: An Analysis of Mutational Reversion. *Genetics* **1994**, *138*, 709-720.

43. Joliot, A.; Pernelle, C.; Deagostini-Bazin, H.; Prochiantz, A. Antennapedia homeobox peptide regulates neural morphogenesis. *Proc. Natl. Acad. Sci. U. S. A.* **1991**, *88*, 1864-1868.

44. Le Roux, I.; Joliot, A. H.; Bloch-Gallego, E.; Prochiantz, A.; Volovitch, M. Neurotrophic activity of the Antennapedia homeodomain depends on its specific DNA-binding properties. *Proc. Natl. Acad. Sci. U. S. A.* **1993**, *90*, 9120-9124.

45. Daff, S.; Sagami, I.; Shimizu, T. The 42-amino acid insert in the FMN domain of neuronal nitric-oxide synthase exerts control over Ca(2+)/calmodulin-dependent electron transfer. *J. Biol. Chem.* **1999**, *274*, 30589-30595.

46. Chin, D.; Means, A. R. Calmodulin: a prototypical calcium sensor. *Trends Cell Biol.* **2000**, *10*, 322-328.

47. Anderson, M. E. Calmodulin kinase signaling in heart: an intriguing candidate target for therapy of myocardial dysfunction and arrhythmias. *Pharmacol. Ther.* **2005**, *106*, 39-55.

48. Chinpongpanich, A.; Wutipraditkul, N.; Thairat, S.; Buaboocha, T. Biophysical characterization of calmodulin and calmodulin-like proteins from rice, Oryza sativa L. *Acta Biochim Biophys Sin (Shanghai)* **2011**, *43*, 867-876.

49. Hoeflich, K. P.; Ikura, M. Calmodulin in Action: Diversity in Target Recognition and Activation Mechanisms. *Cell* **2002**, *108*, 739-742.

50. Bredt, D. S.; Snyder, S. H. Isolation of nitric oxide synthetase, a calmodulin-requiring enzyme. *Proc. Natl. Acad. Sci. U. S. A.* **1990**, *87*, 682-685.

51. Stuehr, D. J.; Cho, H. J.; Kwon, N. S.; Weise, M. F.; Nathan, C. F. Purification and characterization of the cytokine-induced macrophage nitric oxide synthase: an FAD- and FMN-containing flavoprotein. *Proc. Natl. Acad. Sci. U. S. A.* **1991**, *88*, 7773-7777.

52. Fleming, I.; Busse, R. Signal transduction of eNOS activation. *Cardiovasc. Res.* **1999**, *43*, 532-541.

53. Busse, R.; Mülsch, A. Calcium-dependent nitric oxide synthesis in endothelial cytosol is mediated by calmodulin. *FEBS Lett.* **1990**, *265*, 133-136.

54. Cho, H. J.; Xie, Q. W.; Calaycay, J.; Mumford, R. A.; Swiderek, K. M.; Lee, T. D.; Nathan, C. Calmodulin is a subunit of nitric oxide synthase from macrophages. *J. Exp. Med.* **1992**, *176*, 599-604.

55. Zhou, L.; Zhu, D. Y. Neuronal nitric oxide synthase: structure, subcellular localization, regulation, and clinical implications. *Nitric Oxide* **2009**, *20*, 223-230.

56. Boissel, J. P.; Schwarz, P. M.; Forstermann, U. Neuronal-type NO synthase: transcript diversity and expressional regulation. *Nitric Oxide* **1998**, *2*, 337-349.

57. McMurry, J. L.; Chrestensen, C. A.; Scott, I. M.; Lee, E. W.; Rahn, A. M.; Johansen, A. M.; Forsberg, B. J.; Harris, K. D.; Salerno, J. C. Rate, affinity and calcium dependence of nitric oxide synthase isoform binding to the primary physiological regulator calmodulin. *FEBS J.* **2011**, *278*, 4943-4954.

58. Engebrecht, J.; Silverman, M. Identification of genes and gene products necessary for bacterial bioluminescence. *Proc. Natl. Acad. Sci. U. S. A.* **1984**, *81*, 4154-4158.

59. Miroux, B.; Walker, J. E. Over-production of Proteins inEscherichia coli: Mutant Hosts that Allow Synthesis of some Membrane Proteins and Globular Proteins at High Levels. *J. Mol. Biol.* **1996**, *260*, 289-298.

60. Zheng, C.; Simcox, T.; Xu, L.; Vaillancourt, P. A new expression vector for high level protein production, one step purification and direct isotopic labeling of calmodulin-binding peptide fusion proteins. *Gene* **1997**, *186*, 55-60.

61. Roman, L. J.; Sheta, E. A.; Martasek, P.; Gross, S. S.; Liu, Q.; Masters, B. S. High-level expression of functional rat neuronal nitric oxide synthase in Escherichia coli. *Proc. Natl. Acad. Sci. U. S. A.* **1995**, *92*, 8428-8432.

62. Gerber, N. C.; Ortiz de Montellano, P. R. Neuronal nitric oxide synthase. Expression in Escherichia coli, irreversible inhibition by phenyldiazene, and active site topology. *J. Biol. Chem.* **1995**, *270*, 17791-17796.

63. Mondragon, A.; Griffith, E. C.; Sun, L.; Xiong, F.; Armstrong, C.; Liu, J. O. Overexpression and purification of human calcineurin alpha from Escherichia coli and assessment of catalytic functions of residues surrounding the binuclear metal center. *Biochemistry* **1997**, *36*, 4934-4942.

64. Wei, Q.; Lee, E. Y. Expression and reconstitution of calcineurin A and B subunits. *Biochem. Mol. Biol. Int.* **1997**, *41*, 169-177.

65. Hemenway, C. S.; Heitman, J. Calcineurin. Structure, function, and inhibition. *Cell Biochem. Biophys.* **1999**, *30*, 115-151.

66. Huang, Y.; Liu, Z. R. The ATPase, RNA unwinding, and RNA binding activities of recombinant p68 RNA helicase. *J. Biol. Chem.* **2002**, *277*, 12810-12815.

67. Wang, H.; Gao, X.; Yang, J. J.; Liu, Z. R. Interaction between p68 RNA helicase and Ca2+-calmodulin promotes cell migration and metastasis. *Nat. Commun.* **2013**, *4*, 1354.

68. Xie, C.; Zhang, Y.; Wang, H. H.; Matsumoto, A.; Nakamura, A.; Ishikawa, R.; Yoshiyama, S.; Hayakawa, K.; Kohama, K.; Gao, Y. Calcium regulation of non-kinase and kinase activities of recombinant myosin light-chain kinase and its mutants. *IUBMB Life* **2009**, *61*, 1092-1098.

69. Bachs, O.; Lanini, L.; Serratosa, J.; Coll, M. J.; Bastos, R.; Aligue, R.; Rius, E.; Carafoli, E. Calmodulin-binding proteins in the nuclei of quiescent and proliferatively activated rat liver cells. *J. Biol. Chem.* **1990**, *265*, 18595-18600.

70. Zhang, D. Q.; Wang, Y. P.; Wang, W. H.; Sui, X. M.; Jiang, J. Q.; Jiang, X. M.; Xu, Z. S.; Liu, Y. G. Interaction between protein 4.1R and spectrin heterodimers. *Mol. Med. Rep.* **2011**, *4*, 651-654.

71. Lillemoen, J.; Hoffman, D. W. An investigation of the dynamics of ribosomal protein L9 using heteronuclear NMR relaxation measurements1. *J. Mol. Biol.* **1998**, *281*, 539-551.

72. Berggard, T.; Arrigoni, G.; Olsson, O.; Fex, M.; Linse, S.; James, P. 140 mouse brain proteins identified by Ca2+-calmodulin affinity chromatography and tandem mass spectrometry. *J. Proteome Res.* **2006**, *5*, 669-687.

73. O'Connell, D.,J.; Bauer, M. C.; O'Brien, J.; Johnson, W. M.; Divizio, C. A.; O'Kane, S.,L.; BerggÃ¥rd, T.; Merino, A.; â„«kerfeldt, K.,S.; Linse, S.; Cahill, D. J. Integrated Protein Array Screening and High Throughput Validation of 70 Novel

Neural Calmodulin-binding Proteins. *Molecular & Cellular Proteomics : MCP* **2009**, *9*, 1118-1132.

74. VYSOTSKAYA, V.; TISCHENKO, S.; GARBER, M.; KERN, D.; MOUGEL, M.; EHRESMANN, C.; EHRESMANN, B. The ribosomal protein S8 from Thermus thermophilus VK1. *European Journal of Biochemistry* **1994**, *223*, 437-445.

75. Lancaster, L.; Culver, G. M.; Yusupova, G. Z.; Cate, J. H.; Yusupov, M. M.; Noller, H. F. The location of protein S8 and surrounding elements of 16S rRNA in the 70S ribosome from combined use of directed hydroxyl radical probing and X-ray crystallography. *RNA* **2000**, *6*, 717-729.

76. Zhang, J.; Chan, E. K. L.; Peng, X.; Tan, E. M. A Novel Cytoplasmic Protein with RNA-binding Motifs Is an Autoantigen in Human Hepatocellular Carcinoma. *J. Exp. Med.* **1999**, *189*, 1101-1110.

77. Portoles, M.; Faura, M.; Renau-Piqueras, J.; Iborra, F. J.; Saez, R.; Guerri, C.; Serratosa, J.; Rius, E.; Bachs, O. Nuclear calmodulin/62 kDa calmodulin-binding protein complexes in interphasic and mitotic cells. *J. Cell. Sci.* **1994**, *107 (Pt 12)*, 3601-3614.

78. Cormier, M. J.; Charbonneau, H.; Jarrett, H. W. Plant and fungal calmodulin: Ca2+-dependent regulation of plant NAD kinase. *Cell Calcium* **1981**, *2*, 313-331.

79. Epel, D.; Patton, C.; Wallace, R. W.; Cheung, W. Y. Calmodulin activates NAD kinase of sea urchin eggs: an early event of fertilization. *Cell* **1981**, *23*, 543-549.

80. Tunnemann, G.; Martin, R. M.; Haupt, S.; Patsch, C.; Edenhofer, F.; Cardoso, M. C. Cargo-dependent mode of uptake and bioavailability of TAT-containing proteins and peptides in living cells. *FASEB J.* **2006**, *20*, 1775-1784.

81. Madani, F.; Lindberg, S.; Langel, U.; Futaki, S.; Graslund, A. Mechanisms of cellular uptake of cell-penetrating peptides. *J. Biophys.* **2011**, *2011*, 414729.

82. Derossi, D.; Calvet, S.; Trembleau, A.; Brunissen, A.; Chassaing, G.; Prochiantz, A. Cell Internalization of the Third Helix of the Antennapedia Homeodomain Is Receptor-independent. *Journal of Biological Chemistry* **1996**, *271*, 18188-18193.

83. Herce, H. D.; Garcia, A. E. Molecular dynamics simulations suggest a mechanism for translocation of the HIV-1 TAT peptide across lipid membranes. *Proceedings of the National Academy of Sciences* **2007**, *104*, 20805-20810.

84. Pouny, Y.; Rapaport, D.; Mor, A.; Nicolas, P.; Shai, Y. Interaction of antimicrobial dermaseptin and its fluorescently labeled analogues with phospholipid membranes. *Biochemistry* **1992**, *31*, 12416-12423.

85. Lonn, P.; Dowdy, S. F. Cationic PTD/CPP-mediated macromolecular delivery: charging into the cell. *Expert Opin. Drug Deliv.* **2015**, *12*, 1627-1636.

86. Commisso, C.; Davidson, S. M.; Soydaner-Azeloglu, R.; Parker, S. J.; Kamphorst, J. J.; Hackett, S.; Grabocka, E.; Nofal, M.; Drebin, J. A.; Thompson, C. B.; Rabinowitz, J. D.; Metallo, C. M.; Heiden, M. G. V.; Bar-Sagi, D. Macropinocytosis of protein is an amino acid supply route in Ras-transformed cells. *Nature* **2013**, *497*, 10.1038/nature12138.

87. Matsubara, M.; Hayashi, N.; Titani, K.; Taniguchi, H. Circular dichroism and 1H NMR studies on the structures of peptides derived from the calmodulin-binding domains of inducible and endothelial nitric-oxide synthase in solution and in complex with calmodulin. Nascent alpha-helical structures are stabilized by calmodulin both in the presence and absence of Ca2+. *J. Biol. Chem.* **1997**, *272*, 23050-23056.

88. McMahon, H. T.; Boucrot, E. Molecular mechanism and physiological functions of clathrin-mediated endocytosis. *Nature Reviews Molecular Cell Biology* **2011**, 517.

89. Pelkmans, L.; Helenius, A. Endocytosis Via Caveolae. *Traffic* **2002**, *3*, 311-320.

90. Rejman, J.; Oberle, V.; Zuhorn, I. S.; Hoekstra, D. Size-dependent internalization of particles via the pathways of clathrin- and caveolae-mediated endocytosis. *Biochem. J.* **2004**, *377*, 159-169.

91. Hansen, C. G.; Nichols, B. J. Molecular mechanisms of clathrin-independent endocytosis. *J. Cell. Sci.* **2009**, *122*, 1713-1721.

92. Juers, D. H.; Heightman, T. D.; Vasella, A.; McCarter, J. D.; Mackenzie, L.; Withers, S. G.; Matthews, B. W. A structural view of the action of Escherichia coli (lacZ) beta-galactosidase. *Biochemistry* **2001**, *40*, 14781-14794.

93. Ohto, U.; Usui, K.; Ochi, T.; Yuki, K.; Satow, Y.; Shimizu, T. Crystal structure of human beta-galactosidase: structural basis of Gm1 gangliosidosis and morquio B diseases. *J. Biol. Chem.* **2012**, *287*, 1801-1812.

94. Laberge, M.; Huang, Q.; Schweitzer-Stenner, R.; Fidy, J. The Endogenous Calcium Ions of Horseradish Peroxidase C Are Required to Maintain the Functional Nonplanarity of the Heme. *Biophys. J.* **2003**, *84*, 2542-2552.

95. Veitch, N. C. Horseradish peroxidase: a modern view of a classic enzyme. *Phytochemistry* **2004**, *65*, 249-259.

96. Utashima, Y.; Matsumoto, H.; Masaki, K.; Iefuji, H. Heterologous production of horseradish peroxidase C1a by the basidiomycete yeast Cryptococcus sp. S-2 using codon and signal optimizations. *Appl. Microbiol. Biotechnol.* **2014**, *98*, 7893-7900.

97. Ordway, G. A.; Garry, D. J. Myoglobin: an essential hemoprotein in striated muscle. *J. Exp. Biol.* **2004***, 207*, 3441-3446.

98. Flonta, S. E.; Arena, S.; Pisacane, A.; Michieli, P.; Bardelli, A. Expression and Functional Regulation of Myoglobin in Epithelial Cancers. *The American Journal of Pathology* **2009***, 175*, 201-206.

99. Kanatous, S. B.; Mammen, P. P. A. Regulation of myoglobin expression. *J. Exp. Biol.* **2010***, 213*, 2741-2747.

100. Kirsch, T.; Boehm, M.; Schuckert, O.; Metzger, A. U.; Willbold, D.; Frank, R. W.; Rosch, P. Cloning, high-yield expression in Escherichia coli, and purification of biologically active HIV-1 Tat protein. *Protein Expr. Purif.* **1996***, 8*, 75-84.

101. Greenfield, N. J. Using circular dichroism spectra to estimate protein secondary structure. *Nature protocols* **2006***, 1*, 2876-2890.

102. Lin, K.; Yang, H.; Gao, Z.; Li, F.; Yu, S. Overestimated accuracy of circular dichroism in determining protein secondary structure. *European Biophysics Journal* **2013***, 42*, 455-461.

103. Kelly, S. M.; Price, N. C. The use of circular dichroism in the investigation of protein structure and function. *Curr. Protein Pept. Sci.* **2000***, 1*, 349-384.

104. Holzwarth, G.; Doty, P. The Ultraviolet Circular Dichroism of Polypeptides1. *J. Am. Chem. Soc.* **1965***, 87*, 218-228.

105. Greenfield, N. J.; Fasman, G. D. Computed circular dichroism spectra for the evaluation of protein conformation. *Biochemistry (N. Y.)* **1969***, 8*, 4108-4116.

106. Venyaminov, S. Y.; Baikalov, I. A.; Shen, Z. M.; Wu, C. S. C.; Yang, J. T. Circular Dichroic Analysis of Denatured Proteins: Inclusion of Denatured Proteins in the Reference Set. *Anal. Biochem.* **1993***, 214*, 17-24.

107. O'Day, D. H. CaMBOT: profiling and characterizing calmodulin-binding proteins. *Cell. Signal.* **2003***, 15*, 347-354.

108. Cai, D.; Ren, L.; Zhao, H.; Xu, C.; Zhang, L.; Yu, Y.; Wang, H.; Lan, Y.; Roberts, M. F.; Chuang, J. H.; Naughton, M. J.; Ren, Z.; Chiles, T. C. A molecular-imprint nanosensor for ultrasensitive detection of proteins. *Nature Nanotechnology* **2010***, 5*, 597-601.

109. Wilson, J. L.; Scott, I. M.; McMurry, J. L. Optical biosensing: Kinetics of protein A-IGG binding using biolayer interferometry. *Biochem. Mol. Biol. Educ.* **2010***, 38*, 400-407.

110. Carlsson, K.; Danielsson, P. E.; Liljeborg, A.; MajlÃ¶f, L.; Lenz, R.; Ã…slund, N. Three-dimensional microscopy using a confocal laser scanning microscope. *Opt. Lett.* **1985**, *10*, 53-55.

111. Silvagno, F.; Xia, H.; Bredt, D. S. Neuronal nitric-oxide synthase-mu, an alternatively spliced isoform expressed in differentiated skeletal muscle. *J. Biol. Chem.* **1996**, *271*, 11204-11208.

112. Erazo-Oliveras, A.; Muthukrishnan, N.; Baker, R.; Wang, T.; Pellois, J. Improving the Endosomal Escape of Cell-Penetrating Peptides and Their Cargos: Strategies and Challenges. *Pharmaceuticals* **2012**, *5*, 1177-1209.

113. Salerno, J. C.; Ngwa, V. M.; Nowak, S. J.; Chrestensen, C. A.; Healey, A. N.; McMurry, J. L. Novel cell penetrating peptide-adaptors effect intracellular delivery and endosomal escape of protein cargos. *J. Cell. Sci.* **2016**.

114. Zorko, M.; Langel, Ü Cell-penetrating peptides: mechanism and kinetics of cargo delivery. *Adv. Drug Deliv. Rev.* **2005**, *57*, 529-545.

115. Foster, L. J.; de Hoog, C. L.; Zhang, Y.; Zhang, Y.; Xie, X.; Mootha, V. K.; Mann, M. A Mammalian Organelle Map by Protein Correlation Profiling. *Cell* **2006**, *125*, 187-199.

116. Morris, M. C.; Chalion, L.; Heitz, F.; Divita, G. Signal sequence based Cell Penetratine Peptides and theirs applications for gene delivery. *Cell Penetrating peptides: Processes and application* **2002**.

117. Alberts, B.; Johnson, A.; Lewis, J.; et al., Eds.; In *Molecular Biology of the Cell: The Endoplasmic Reticulum.* Garland Science: New York:, 2002; Vol. 4th edition.

118. Torchilin, V. Intracellular delivery of protein and peptide therapeutics. *Drug Discovery Today: Technologies* **2008**, *5*, e95-e103.

119. - Stewart, K. M.; - Horton, K. L.; - Kelley, S. O. - Cell-penetrating peptides as delivery vehicles for biology and medicine. - *Org. Biomol. Chem.* , - 2242.

120. Regberg,Jakob; Srimanee,Artita; Langel,Ãœlo .

121. Rousselle, C.; Clair, P.; Lefauconnier, J. M.; Kaczorek, M.; Scherrmann, J. M.; Temsamani, J. New advances in the transport of doxorubicin through the blood-brain barrier by a peptide vector-mediated strategy. *Mol. Pharmacol.* **2000**, *57*, 679-686.

122. Lindgren, M.; Rosenthal-Aizman, K.; Saar, K.; Eiríksdóttir, E.; Jiang, Y.; Sassian, M.; Östlund, P.; Hällbrink, M.; Langel, Ü Overcoming methotrexate resistance in breast cancer tumour cells by the use of a new cell-penetrating peptide. *Biochem. Pharmacol.* **2006**, *71*, 416-425.

123. Powers, E. T.; Morimoto, R. I.; Dillin, A.; Kelly, J. W.; Balch, W. E. Biological and chemical approaches to diseases of proteostasis deficiency. *Annu. Rev. Biochem.* **2009**, *78*, 959-991.

124. Han, J.; Lee, J. D.; Bibbs, L.; Ulevitch, R. J. A MAP kinase targeted by endotoxin and hyperosmolarity in mammalian cells. *Science* **1994**, *265*, 808-811.

125. ZARUBIN, T.; HAN, J. Activation and signaling of the p38 MAP kinase pathway. *Cell Res.* **2005**, *15*, 11-18.

126. Wagner, E. F.; Nebreda, A. R. Signal integration by JNK and p38 MAPK pathways in cancer development. *Nat. Rev. Cancer.* **2009**, *9*, 537-549.

127. Cardozo, A. K.; Buchillier, V.; Mathieu, M.; Chen, J.; Ortis, F.; Ladrière, L.; Allaman-Pillet, N.; Poirot, O.; Kellenberger, S.; Beckmann, J. S.; Eizirik, D. L.; Bonny, C.; Maurer, F. Cell-permeable peptides induce dose- and length-dependent cytotoxic effects. *Biochimica et Biophysica Acta (BBA) - Biomembranes* **2007**, *1768*, 2222-2234.